JEM Journal of Experimental Medicine

BRIEF DEFINITIVE REPORT

Endothelial mTOR maintains hematopoiesis during aging

Pradeep Ramalingam[1], Michael G. Poulos[2], Michael C. Gutkin[2], Lizabeth Katsnelson[1], Ana G. Freire[2], Elisa Lazzari[2], and Jason M. Butler[1,2,3]

Aging leads to a decline in hematopoietic stem and progenitor cell (HSPC) function. We recently discovered that aging of bone marrow endothelial cells (BMECs) leads to an altered crosstalk between the BMEC niche and HSPCs, which instructs young HSPCs to behave as aged HSPCs. Here, we demonstrate aging leads to a decrease in mTOR signaling within BMECs that potentially underlies the age-related impairment of their niche activity. Our findings reveal that pharmacological inhibition of mTOR using Rapamycin has deleterious effects on hematopoiesis. To formally determine whether endothelial-specific inhibition of mTOR can influence hematopoietic aging, we conditionally deleted mTOR in ECs (mTOR$^{(ECKO)}$) of young mice and observed that their HSPCs displayed attributes of an aged hematopoietic system. Transcriptional profiling of HSPCs from mTOR$^{(ECKO)}$ mice revealed that their transcriptome resembled aged HSPCs. Notably, during serial transplantations, exposure of wild-type HSPCs to an mTOR$^{(ECKO)}$ microenvironment was sufficient to recapitulate aging-associated phenotypes, confirming the instructive role of EC-derived signals in governing HSPC aging.

Introduction

The number of elderly is increasing with unprecedented speed around the globe. The aging process is associated with an increased susceptibility to cardiovascular and hematopoietic disorders. Aging is associated with increased risk of negative outcomes/treatment failures because elderly patients respond poorly to myeloablative strategies that are necessary for the successful transplantation of hematopoietic stem and progenitor cells (HSPCs) and also develop prolonged cytopenias following myelosuppressive therapies that are often used to treat hematopoietic malignancies and other cancers (Balducci, 2003). One of the most significant changes observed during the aging process is a decline in the overall function of endothelial cells (ECs), including the EC niche of the hematopoietic system (Das et al., 2018; El Assar et al., 2012; Le Couteur and Lakatta, 2010). An increasing body of evidence demonstrating functional interactions between the HSPC and its niche suggests that both local and systemic factors regulate HSPC function (Bowers et al., 2018; Crane et al., 2017; Decker et al., 2018; Lazzari and Butler, 2018; Pinho and Frenette, 2019). However, to date, most reports describing alterations in the aged hematopoietic compartment have focused on the cell-intrinsic properties of HSPCs. For instance, it has been demonstrated that whereas the absolute number of immunophenotypically defined HSPCs increases with age, aged HSPCs exhibit a decrease in their long-term reconstitution abilities (Chambers et al., 2007; Geiger et al., 2013; Kowalczyk et al., 2015; Pang et al., 2011; Rossi et al., 2005) and show a significant myeloid bias at the expense of lymphopoiesis (Cho et al., 2008; Dykstra and de Haan, 2008; Rossi et al., 2005; Van Zant and Liang, 2003). In contrast, the role of the aged microenvironment—specifically aged bone marrow ECs (BMECs)—in regulating HSPC function during aging has been far less examined.

It has been shown that BMECs assume an instructive role in supporting HSPC self-renewal and differentiation into lineage-committed progeny, in part mediated by activation of their AKT signaling pathway (Butler et al., 2010; Poulos et al., 2015). When interrogating signaling pathways downstream of AKT, we found that the mechanistic target of Rapamycin (mTOR) signaling pathway stimulated the expression of pro-HSPC paracrine factors within AKT-activated ECs (Kobayashi et al., 2010). The mTOR complex utilizes many signals, including growth factors and oxygen tension, to regulate cell growth, proliferation, protein synthesis, energy metabolism, and survival (Zoncu et al., 2011). mTOR activity is strongly linked to physiological aging, and inhibiting mTOR activity increases the longevity of aged mice (Harrison et al., 2009; Inoki et al., 2003; Kaeberlein et al., 2005; Kapahi et al., 2004; Lee et al., 2010; Vellai et al., 2003; Wullschleger et al., 2006). Physiological aging of the HSPC pool

[1]Department of Medicine, Division of Regenerative Medicine, Weill Cornell Medical College, New York, NY; [2]Center for Discovery and Innovation, Hackensack University Medical Center, Nutley, NJ; [3]Molecular Oncology Program, Georgetown University, Washington, DC.

Correspondence to Jason M. Butler: Jason.Butler@hmh-cdi.org.

is also regulated by mTOR activity, and it has been reported that the mTOR pathway is dysregulated in aged mice and that increased mTOR activation within HSPCs results in their depletion (Chen et al., 2009). However, the regulation of HSPC activity by mTOR signaling in the aged bone marrow (BM) endothelial niche and its contribution to the aging of the hematopoietic system have not been studied.

We recently demonstrated that aged BMECs can instruct young HSPCs to function as aged HSPCs, whereas young BMECs can preserve the functional output of aged HSPCs (Poulos et al., 2017). Upon further examination of the pathways regulating BMEC niche function, we found that physiological aging is associated with decreased AKT/mTOR signaling within BMECs, which potentially impairs their niche activity. In support of this hypothesis, we observed that pharmacological inhibition of mTOR signaling in aged mice by Rapamycin treatment resulted in an increase in hematopoietic aging phenotypes at homeostasis and severe defects in the hematopoietic system following myelosuppression. Furthermore, EC-specific deletion of mTOR in young mice resulted in premature aging of the hematopoietic system, where many of the phenotypic and functional attributes of HSPCs from EC mTOR knockout ($mTOR^{(ECKO)}$) mice closely resembled those of aged mice. Together, these studies have identified BMECs and AKT/mTOR signaling as key components in regulating HSPC self-renewal and differentiation during the aging process.

Results and discussion

To determine whether physiological aging alters mTOR signaling within the BM, we performed immunoblot analysis in whole BM (WBM) cells, which revealed that aging is associated with a decreased expression of mTOR signaling targets, including phospho-S6 and phospho-4EBP-1 (Fig. S1, A and B). Phosphoflow analysis demonstrated a decreased expression of phospho-mTOR, phospho-S6, and phospho-Akt in both $lineage^{-}CD45^{+}$ HSPCs and BMECs of aged mice (Fig. S1, C and D), confirming that aging is associated with decreased mTOR signaling within the BM microenvironment.

Genetic inhibition of mTOR signaling has been demonstrated to improve life span and have rejuvenating effects in many model systems (Kennedy and Lamming, 2016). Indeed, it has been suggested that inhibition of mTOR signaling by Rapamycin treatment can rejuvenate aged HSPC function (Chen et al., 2009). Contrarily, treatment of cancer patients with mTOR inhibitors is associated with infections and hematological toxicities (Rafii et al., 2015; Xu and Tian, 2014) and usage of sirolimus in graft-versus-host disease (GVHD) prophylaxis has been associated with hematological insufficiencies and vasculopathy (Cutler et al., 2005; Lutz and Mielke, 2016). To address these dichotomous findings, we set out to comprehensively determine the effects of mTOR inhibition on aging hematopoiesis. To this end, we treated 24-mo-old mice with control feed or feed impregnated with 14 parts per million (PPM) of Rapamycin for 2 wk to evaluate their hematopoietic parameters (Fig. 1 A). The 14-PPM feed has been shown to maintain plasma concentration of ∼3–5 ng/ml in C57BL/6 mice, which is similar to the therapeutic target levels for GVHD prophylaxis (∼3–12 ng/ml) and is considered to be a "low-dose" regimen for mouse longevity and rejuvenation studies (Fok et al., 2014; Johnson et al., 2015; Neff et al., 2013; Zhang et al., 2014). Immunoblot analysis of WBM cells isolated from Rapamycin-treated mice demonstrated a decreased expression of phospho-S6 and phospho-4EBP-1 consistent with mTOR inhibition (Fig. S1, E and F). The modest reduction in expression of phospho-S6 is consistent with a previously reported level of inhibition in aged C57BL/6 mice treated with a 14-PPM diet (Zhang et al., 2014) and is likely due to the low dose of Rapamycin and the decreased basal expression of these phospho-proteins within the aged BM. Despite the modest reduction in mTOR signaling following Rapamycin, complete blood counts demonstrated that Rapamycin-treated aged mice had significant decreases in white blood cell (WBC) and platelet counts (Fig. 1 B). Interestingly, the decrease in total WBC counts was associated with an increased frequency of myeloid cells and a decrease in T cells, likely mediated in part by the direct toxicity of Rapamycin on T cells (Molhoek et al., 2009; Tian et al., 2004; Fig. 1 C). Total cells per femur and the frequency of phenotypic HSPCs were not affected with Rapamycin treatment (Fig. 1, D and E). However, functional assays for assessing progenitor potential and HSPC activity revealed significant disruption in hematopoiesis. Progenitor activity assessed by CFU assay revealed that Rapamycin-treated mice displayed a significant decrease in progenitor activity (Fig. 1 F).

We next examined the long-term repopulation potential of HSPCs in a competitive BM transplantation assay, where 5×10^5 WBM cells isolated from Rapamycin-treated or control aged mice (CD45.2) were competitively transplanted along with 5×10^5 CD45.1 WBM cells into lethally irradiated CD45.1 mice. BM cells from Rapamycin-treated mice demonstrated a decrease in engraftment potential with a myeloid-biased output at the expense of lymphocytes, confirming a direct effect of Rapamycin at the level of HSPCs (Fig. 1, G–I). These data suggest that systemic mTOR inhibition results in an increase in the functional defects observed in the hematopoietic system of aged mice.

Aberrant mTOR activation has been observed in a wide spectrum of hematological cancers as well as solid tumors, and mTOR inhibitors are currently being evaluated as a stand-alone or as an adjuvant to standard chemotherapy regimens (Calimeri and Ferreri, 2017; Huang et al., 2015). The immunosuppressive properties of mTOR inhibitors are widely used to prevent GVHD following allogenic hematopoietic stem cell transplantation (HSCT; Armand et al., 2016; Cutler and Antin, 2010). Chemoradiation-based conditioning regimens for HSCT as well as standard induction regimens for hematological malignancies are often associated with cytopenias resulting from the myelosuppressive injury of the endogenous HSPCs. Prior studies have shown that HSPCs undergo mTOR activation during myelosuppressive recovery (Baumgartner et al., 2018) and that mTORC1 inhibition delays hematopoietic recovery (Yan et al., 2016).

To determine the impact of mTOR inhibition on regeneration of aged HSPCs, we subjected aged mice to sublethal irradiation (650 Rad) or chemotherapy (Ara-C 100 mg/kg 5 d and doxorubicin [Doxo] 3 mg/kg 3 d) and maintained the mice on either

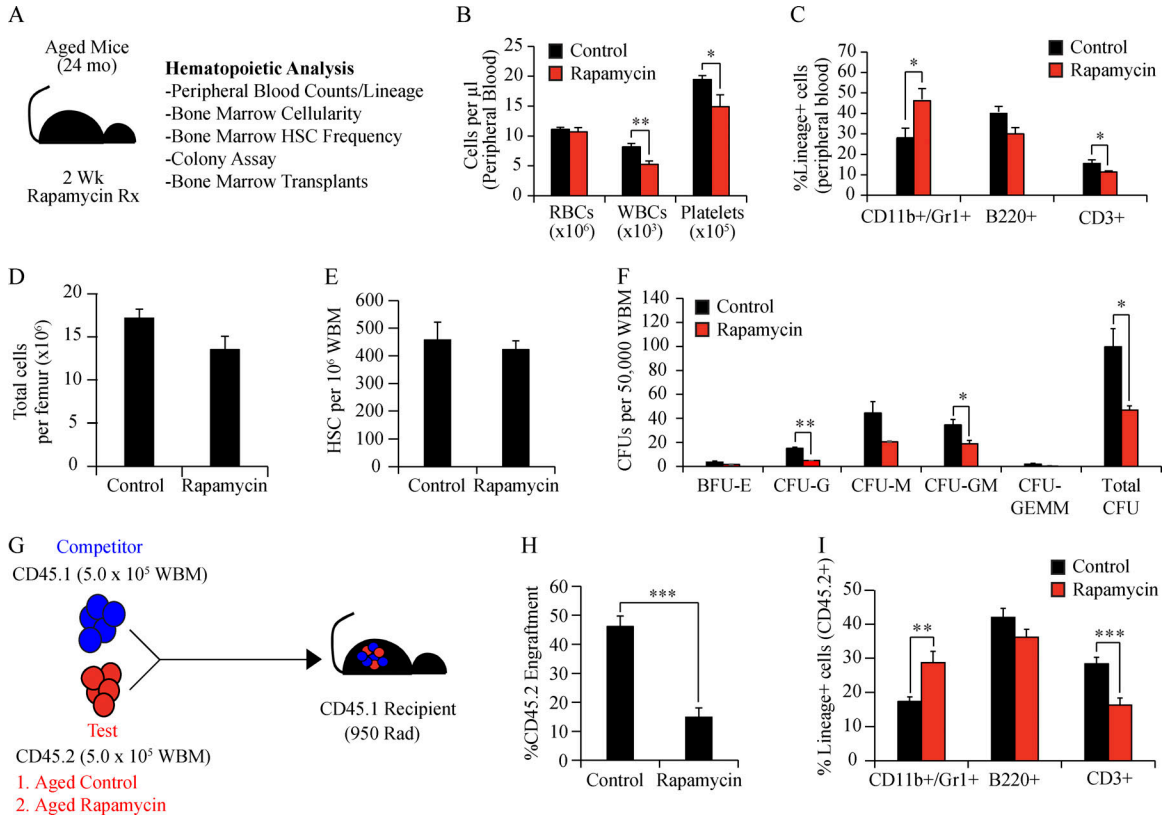

Figure 1. **Rapamycin adversely impacts hematopoiesis and HSPC activity in aged mice. (A)** Experimental design to assess the impact of Rapamycin treatment (Rx) on aging hematopoiesis. **(B)** Bar graphs of peripheral blood counts demonstrating a decrease in WBC and platelets following Rapamycin treatment (n = 12 mice per cohort). **(C)** Lineage composition of peripheral blood CD45⁺ cells showing an increased frequency of myeloid cells in Rapamycin-treated aged mice (n = 8–10 mice per cohort). **(D and E)** Total hematopoietic cells (n = 12 mice per cohort; D) and the frequency of immunophenotypically defined HSCs per femur (n = 8 mice per cohort; E). **(F)** Methylcellulose-based colony assay by quantifying CFUs revealed a decrease in hematopoietic progenitor activity (n = 3 mice per cohort). Note that BFU-E denotes burst-forming unit–erythroid, whereas CFU-G, CFU-M, CFU-GM, and CFU-GEMM denote CFU-granulocyte, CFU-macrophage, CFU-granulocyte/macrophage, and CFU-granulocyte/erythroid/macrophage/megakaryocyte, respectively. Data in B–F represent combined analysis of two independent experiments. **(G)** Schematic of competitive WBM transplantation assay to assess HSPC activity within WBM cells following Rapamycin treatment. **(H and I)** Peripheral blood analysis 16 wk after transplantation revealed a decrease in long-term engraftment potential (H) and myeloid-biased lineage output at the expense of lymphopoiesis (I; n = 10 recipients per cohort), confirming that Rapamycin adversely impacts HSPC activity in aged mice. Data represent average engraftment following transplantation of cells derived from n = 3 independent donor mice per cohort. Error bars represent sample mean ± SEM. Statistical significance determined using Student's t test. *, P < 0.05; **, P < 0.01; ***, P < 0.001.

control diet or Rapamycin-impregnated feed during a 28-d recovery phase (Fig. 2, A and I). Analysis of peripheral blood revealed that Rapamycin-treated mice displayed significant delay in WBC and platelet recovery in both injury models and a delay in neutrophil recovery following chemotherapy, indicating that mTOR signaling supports the recovery of the aged hematopoietic system following both myelosuppressive injuries (Fig. 2, B and J). We next examined whether Rapamycin treatment impacted the number and functional potential of aged HSPCs following the 28-d hematopoietic recovery phase. Both total femur counts and the frequency of phenotypic HSPCs were significantly reduced with Rapamycin treatment, suggesting that mTOR signaling is essential for HSPC recovery and restoration of BM cellularity (Fig. 2, C, D, K, and L). Additionally, Rapamycin treatment significantly affected the progenitor activity of the hematopoietic system, with a significant decrease in progenitor function following chemotherapy and radiation (Fig. 2, E and M).

To test if the decrease in phenotypic HSPCs manifests a decrease in engraftment potential, WBM (CD45.2⁺) cells were isolated from control and Rapamycin-treated groups and were transplanted with a competitive dose of young CD45.1⁺ WBM in a 5:1 ratio into lethally irradiated young CD45.1 recipients (Fig. 2, F and N). Peripheral blood analysis after 16 wk following transplantation revealed a significant decrease in engraftment of transplanted cells from Rapamycin-treated mice from both myelosuppression groups (Fig. 2, G and O), with Rapamycin-treated mice after irradiation resulting in no observable engraftment (Fig. 2 O). Although Rapamycin treatment did not result in significant changes in the lineage composition of the transplanted cells (Fig. 2, H and P), there was a notable increase in the frequency of myeloid cells (Fig. 2 H). These data also demonstrate that irradiation (650 Rad) results in a higher degree of myelosuppressive injury compared with the induction chemotherapy (Ara-C + Doxo) as indicated by the delayed WBC and neutrophil recovery, decreased BM cellularity, and hematopoietic stem cell (HSC) frequency and engraftment potential in aged control mice receiving radiation compared with aged control mice subject to chemotherapy. These findings are similar to

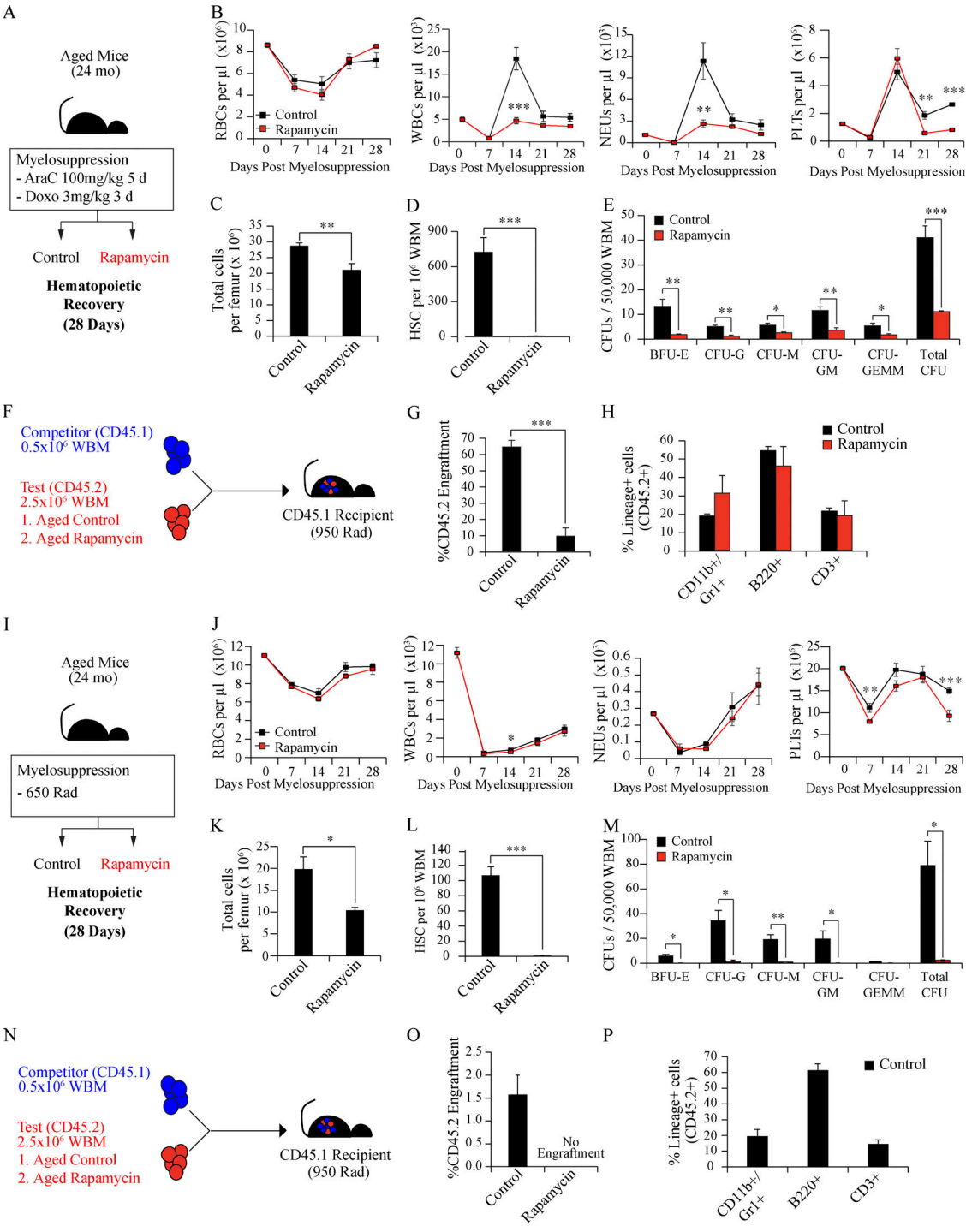

Figure 2. **Rapamycin impairs hematopoietic recovery following myelosuppressive injury. (A)** Experimental design to assess the impact of Rapamycin on hematopoietic recovery following chemotherapy. **(B)** Peripheral blood counts demonstrate a delay in WBC, neutrophil (NEU), and platelet (PLT) recovery following chemotherapy (n = 6 mice per cohort). **(C and D)** Total hematopoietic cells per femur (n = 5 mice per cohort; C) and the frequency of HSCs per 10^6 femur cells (n = 5 mice per cohort; D) at day 28 following chemotherapy. **(E)** Methylcellulose-based colony assay to assess hematopoietic progenitor activity (n = 3 mice per cohort). Data in B–E represent combined analysis of two independent experiments. **(F)** Schematic of competitive WBM transplantation assay to determine HSPC recovery following chemotherapy. **(G and H)** Peripheral blood analysis 16 wk after transplantation revealed a loss of long-term engraftment potential (G) and normal lineage reconstitution (H; n = 6 recipients per cohort) in donor WBM cells derived from Rapamycin-treated mice. Data represent average engraftment following transplantation of WBM cells derived from n = 6 independent donor mice per cohort. **(I)** Experimental design to assess the impact of Rapamycin on hematopoietic recovery following myelosuppressive irradiation. **(J)** Peripheral blood counts demonstrate a delay in WBC and platelet recovery following radiation (n = 11 mice per cohort). **(K and L)** Total hematopoietic cells per femur (n = 5 mice per cohort; K) and the frequency of HSCs per 10^6 femur cells (n = 5 mice per cohort; L) at day 28 following irradiation. **(M)** Methylcellulose-based colony assay to assess hematopoietic progenitor activity (n = 3 mice per cohort). Data in J–M represent combined analysis of two independent experiments. **(N)** WBM transplantation assay. **(O and P)** Peripheral blood analysis 16 wk after transplantation revealed a complete loss of long-term engraftment potential (O) and multilineage reconstitution ability (P; n = 4–8

recipients per cohort) in donor WBM cells derived from Rapamycin-treated mice. Data represent average engraftment following transplantation of cells derived from $n = 4$ independent donor mice per cohort. Error bars represent sample mean ± SEM. Statistical significance determined using Student's t test. *, $P < 0.05$; **, $P < 0.01$; ***, $P < 0.001$.

previous reports demonstrating an earlier recovery of WBC counts in young mice subjected to induction chemotherapy (Ara-C + Doxo; Wunderlich et al., 2013) compared with myelosuppressive irradiation (650 Rad; Poulos et al., 2016, 2017). Taken together, these data suggest that inhibition of mTOR signaling in aged mice results in significant hematopoietic defects at steady state, a delay in hematopoietic recovery, and profound impairment of HSPC function following myelosuppressive injury.

The adverse effects of Rapamycin on hematopoiesis of aged mice likely arises due to a direct effect of mTOR inhibition within HSPCs (Guo et al., 2013) and potentially due to its additional impact on the BMEC niche function. Indeed, it has been reported that Rapamycin can lead to long-term endothelial dysfunction in patients receiving sirolimus-eluting stents (Hofma et al., 2006), and vasculopathy is a limiting toxicity in patients undergoing GVHD prophylaxis following allogenic HSCT (Cutler et al., 2005; Lutz and Mielke, 2016). However, the impact of mTOR inhibition on the ability of the endothelial niche to support HSPC activity has not been studied. Given that aged mice manifest significant hematopoietic defects following Rapamycin treatment, it is likely that enhanced hematological toxicity of aged mice to Rapamycin could be partly mediated by the adverse effects of mTOR inhibition on the vascular endothelium, in addition to the direct effect on HSPCs.

To test whether endothelial mTOR is essential for maintaining niche activity, we deleted *mTOR* specifically within ECs of young adult mice (12–16 wk) by crossing an $mTOR^{fl/fl}$ mouse to a tamoxifen-inducible *cre* transgenic mouse driven by the adult EC-specific VE-cadherin promoter ($mTOR^{(ECKO)}$; Benedito et al., 2009). To rule out the effects of *cre*-mediated toxicity, we first analyzed *Cdh5-creERT2*$^{+}$ mice and observed no significant alterations in their BM cellularity, HSC frequency, or peripheral blood lineage composition compared with their *cre*-negative littermate controls, indicating that endothelial-specific expression of *cre* transgene does not affect hematopoiesis (Fig. S1, G–I). To determine the effect of EC-specific *mTOR* deletion on the regulation of HSPCs and their progeny, we performed hematopoietic analysis on young (12–16 wk) $mTOR^{(ECKO)}$ and young (12–16 wk) control mice. 22–24-mo-old wild-type mice served as aged controls. $mTOR^{(ECKO)}$ mice displayed a significant increase in both total BM hematopoietic cells and the frequency of phenotypic long-term repopulating HSCs, similar to aged controls (Fig. 3, A and B). Peripheral blood analysis for lineage composition revealed a significant increase in myeloid cells in young $mTOR^{(ECKO)}$ mice and aged controls, with decreased levels of B cells compared with young control mice (Fig. 3 C). Notably, heterozygote $mTOR^{fl/+}$*creERT2*$^{+}$ mice did not manifest the HSPC aging phenotypes observed in $mTOR^{(ECKO)}$ mice including increased BM cellularity, HSC frequency, and myeloid-skewed peripheral blood lineage composition, demonstrating that deletion of both alleles of endothelial *mTOR* is essential to induce HSPC aging phenotypes (Fig. S1, J–L). Next, we determined that WBM isolated from $mTOR^{(ECKO)}$ and aged mice displayed a decrease in progenitor activity in a methylcellulose CFU assay (Fig. 3 D). We further analyzed HSCs from $mTOR^{(ECKO)}$ mice for levels of γH2AX foci (Flach et al., 2014) and cell polarity status (Florian et al., 2012). HSCs from $mTOR^{(ECKO)}$ mice and aged controls displayed a significant increase in γH2AX foci and a striking loss of α-Tubulin polarity (Fig. 3, E–H) compared with young control mice. Transcriptional analysis revealed that EC-specific *mTOR* deletion leads to changes in HSC gene expression that cluster with aged HSCs (Fig. 3 I).

To define a robust gene expression signature that characterizes an aged HSC, we compared our microarray data with prior datasets published by Rossi et al. (2005) and Chambers et al. (2007) and identified 10 genes that show significant up-regulated expression with aging (Fig. 3 J). RT–quantitative PCR (RT-qPCR) analysis confirmed an up-regulation of all of the 10 "aging-signature" genes in aged HSCs (Fig. 3 K). Strikingly, $mTOR^{(ECKO)}$ HSCs also displayed a similar up-regulation of the aging-signature genes, as observed in aged HSCs (Fig. 3 K). Taken together, these observations suggest that EC-specific *mTOR* deletion is sufficient to induce premature aging of the HSC and the hematopoietic system during homeostasis.

To verify whether these age-related alterations in $mTOR^{(ECKO)}$ mice are due to direct effects on the HSC, we examined the long-term repopulation capacity of HSCs in a BM transplantation assay. CD45.2^{+} HSCs from young $mTOR^{(ECKO)}$, young control, and aged mice were competitively transplanted into lethally irradiated CD45.1 mice (Fig. 4 A). HSCs from young $mTOR^{(ECKO)}$ mice displayed diminished engraftment and a significant myeloid bias at the expense of T-lymphopoiesis (Fig. 4 B) compared with HSCs from young control mice. Notably, the functional attributes of $mTOR^{(ECKO)}$ HSCs are similar to HSCs from aged mice. To determine whether HSCs from $mTOR^{(ECKO)}$ mice display self-renewal defects, we performed secondary transplantation assays (Fig. 4 C). Additionally, we examined whether a BM endothelial niche devoid of mTOR signaling is sufficient to drive young control HSPCs from primary transplants to functionally behave like aged HSPCs (Fig. 4 C). To this end, we isolated and transplanted WBM from primary recipients (that received 100 HSCs from either young control or $mTOR^{(ECKO)}$ mice) into lethally irradiated young control or young $mTOR^{(ECKO)}$ secondary recipients (Fig. 4 C). WBM from aged-HSC primary recipients was transplanted into young wild-type secondary recipients as an aged secondary transplant control (Fig. 4, D–G; red dashed line represents average values). As anticipated, when transplanted into secondary recipients, WBM from aged-HSC primary recipients displayed further decrease in overall engraftment coupled with a myeloid-biased output (Fig. 4, D–G; red dashed line). As expected, when transplanted into secondary control recipients (Fig. 4, D–G; CNTL:CNTL), WBM isolated from young control primary recipients maintained consistent overall

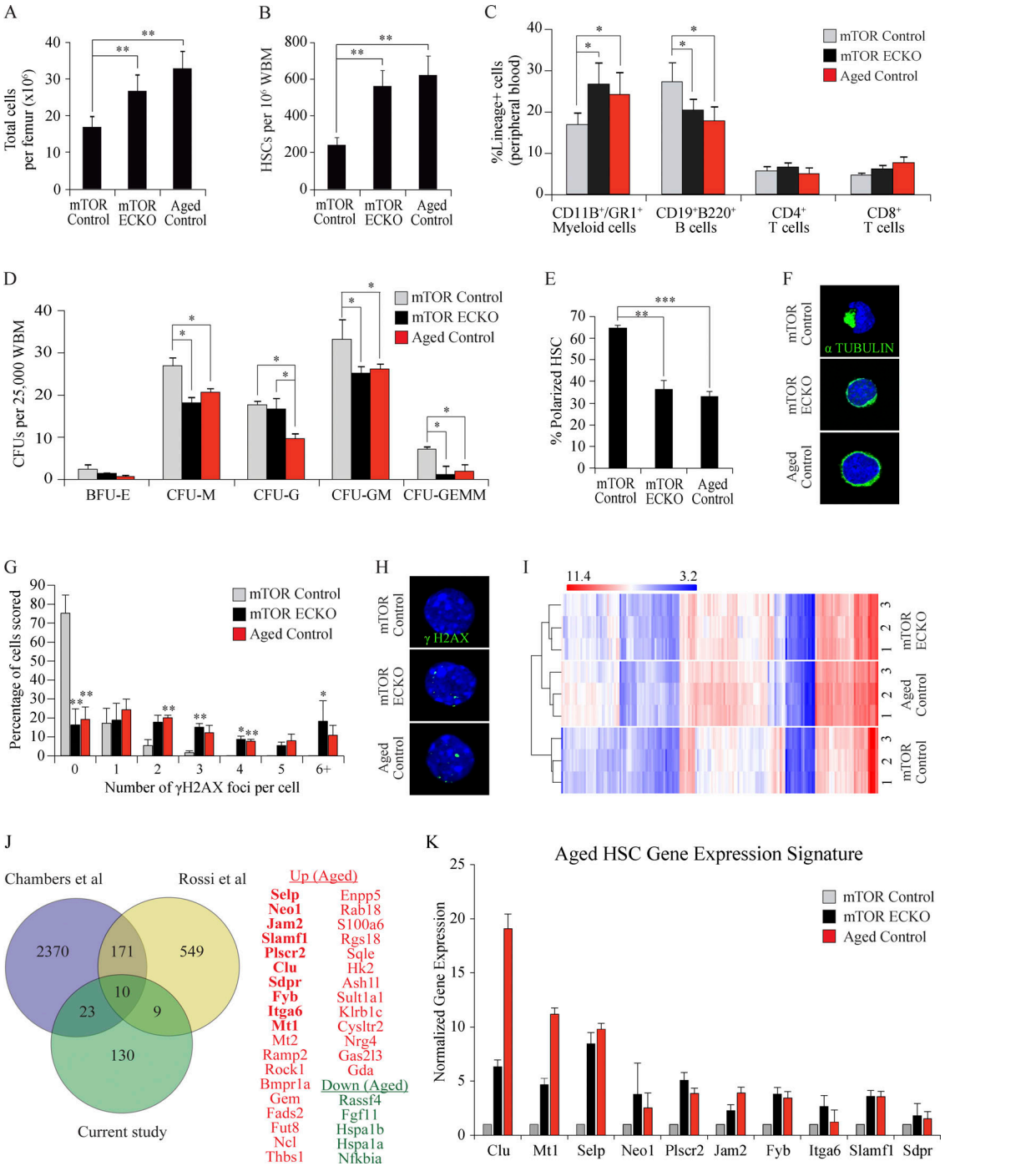

Figure 3. **EC-specific deletion of *mTOR* in young mice leads to aging-related alterations in HSPCs. (A–C)** To determine the effect of endothelial-specific *mTOR* deletion on HSPCs, hematopoietic analysis was performed on young $mTOR^{fl/fl}$ (n = 8), $mTOR^{(ECKO)}$ (n = 10), and aged control mice (n = 5). **(A and B)** Endothelial-specific deletion of *mTOR* resulted in a significant increase in total hematopoietic cells (A) and the frequency of immunophenotypically defined long-term repopulating HSCs (LT-HSCs; B) per femur. **(C)** Lineage composition of $CD45^+$ hematopoietic cells in the peripheral blood. **(D)** Methylcellulose-based colony assay was used to assess hematopoietic progenitor activity by quantifying CFUs (n = 3 mice per cohort). **(E)** Quantification of the frequency of polarized HSCs (n = 3 mice per cohort). **(F)** Representative images of α-Tubulin staining to evaluate HSC cellular polarity. **(G)** Quantification of number of γH2AX foci per HSC (n = 3 mice per cohort). **(H)** Representative images of γH2AX foci in HSC. Data in A–H represent combined analysis of two independent experiments. **(I)** Transcriptional profiling of HSCs by microarray in the indicated genotypes (n = 3 mice per cohort). Note: The phenotypes observed in $mTOR^{(ECKO)}$ mice closely mimic the phenotypes observed in aged control mice. **(J)** Venn diagram comparing genes showing significant changes between young and aged hematopoietic stem cells in the current study and in two previously published datasets. Genes listed demonstrate concordant changes in expression between the current study and published datasets (red, up-regulated in aged HSCs; green, down-regulated in aged HSCs). Genes in bold text were validated by RT-qPCR and represent an aged HSC expression signature. **(K)** RT-qPCR confirmation of microarray-identified aged HSC gene expression signature in $mTOR^{(ECKO)}$ and aged mice (n = 3 mice per cohort). Note: HSCs from $mTOR^{(ECKO)}$ mice share an aged HSC gene expression signature. Error bars represent mean ± SEM. Statistical significance determined using one-way ANOVA with Tukey's correction for multiple comparisons. *, P < 0.05; **, P < 0.01; ***, P < 0.001.

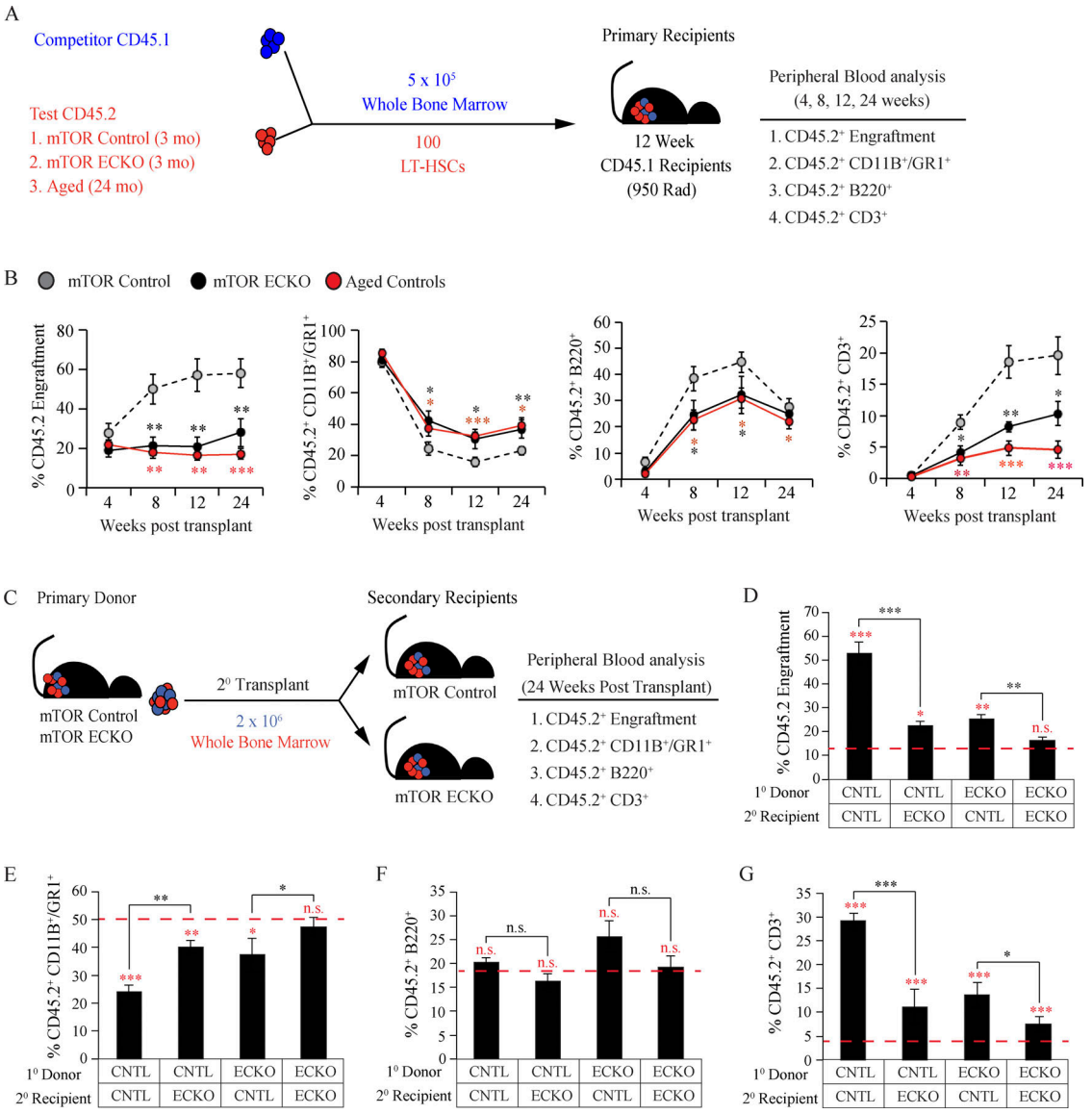

Figure 4. **HSCs from young *mTOR*$^{(ECKO)}$ mice display functional defects resembling aged HSCs. (A)** Schematic of primary transplants. **(B)** Long-term multilineage repopulation capacity of HSCs (n = 10 recipients per cohort). CD45.2$^+$ HSCs transplanted from young *mTOR*$^{(ECKO)}$ mice displayed diminished engraftment potential and a significant myeloid bias at the expense of lymphopoiesis. Data represent average engraftment following transplantation of cells derived from n = 3 independent donor mice per cohort. **(C)** Schematic of secondary transplants. WBM isolated from primary recipients was transplanted into either young *mTOR*$^{fl/fl}$ control or young *mTOR*$^{(ECKO)}$ mice. Primary recipients that received aged HSCs were transplanted into young wild-type secondary-recipient mice and served as aged controls. **(D–G)** Quantification of multilineage engraftment in secondary transplant recipients. CD45.2$^+$ peripheral blood engraftment (D) and myeloid (E), B cell (F), and T cell (G) lineage-committed contribution 24 wk after transplantation (n = 5–7 recipients per cohort). Data represent average engraftment following transplantation of cells derived from n = 5 independent donor mice per cohort. Error bars represent mean ± SEM. Statistical significance determined using Student's t test. *, P < 0.05; **, P < 0.01; ***, P < 0.001. CNTL, control; LT-HSC, long-term repopulating HSC; n.s., not statistically significant.

long-term engraftment and balanced myelo-lymphoid output. However, when transplanted into secondary *mTOR*$^{(ECKO)}$ recipients (Fig. 4, D–G; CNTL:ECKO), WBM isolated from young control primary recipients resulted in a significant decrease in CD45.2 engraftment with the development of a myeloid bias and a decrease in T cell production, confirming that EC-specific deletion of *mTOR* is sufficient to impose aging attributes on HSPCs derived from young control mice. Conversely, transplantation of primary *mTOR*$^{(ECKO)}$ WBM into control secondary recipients (Fig. 4 D; ECKO:CNTL) led to a modest increase in CD45.2 engraftment potential compared with the primary *mTOR*$^{(ECKO)}$ WBM that was transplanted into *mTOR*$^{(ECKO)}$ recipients (Fig. 4 D; ECKO:ECKO). Although a myeloid bias and a decreased T cell output still persisted in the ECKO:CNTL cohort (Fig. 4, E and G), transplanting primary *mTOR*$^{(ECKO)}$ WBM into control recipients (ECKO:CNTL) resulted in a significant reduction in the percentage of myeloid cells and an increase in T cells compared with the ECKO:ECKO cohort (Fig. 4, E and G), suggesting that exposure to a control microenvironment partially restores hematopoietic function. When primary *mTOR*$^{(ECKO)}$ WBM was

transplanted into secondary *mTOR*$^{(ECKO)}$ recipients (Fig. 4 B; ECKO:ECKO), the engraftment was similar to the aged secondary control cohort (Fig. 4 D; red dashed line), with a persisting myeloid bias and decreased T cell output. These data demonstrate that primary control HSPCs can be instructed to assume aging phenotypes following transplantation when introduced into an *mTOR*$^{(ECKO)}$ microenvironment and that partial reversal of the aging phenotypes observed in *mTOR*$^{(ECKO)}$ HSPCs transplanted from primary recipients can be achieved when introduced into a wild-type BM microenvironment.

We next sought to evaluate the roles of mTORC1 and mTORC2 complexes downstream of endothelial mTOR in HSPC regulation. To this end, we generated BM-derived EC lines deficient for Raptor (mTORC1) or Rictor (mTORC2) and used our established co-culture platform (Poulos et al., 2015) to test their impact on HSPC activity (Fig. S2). The functional knockdown of either complex was confirmed by immunoblot analysis for downstream targets of Raptor and Rictor, which demonstrated a decrease in phospho-4EBP-1 upon knockdown of Raptor and a decrease in phospho-Akt upon Rictor knockdown (Fig. S2, A–G). Analysis after 9 d of co-culture revealed no significant differences in total hematopoietic expansion after knockdown of either complex (Fig. S2, H and I). However, colony assays revealed a significant reduction in CFU-forming ability of HSPCs co-cultured on Raptor as well as Rictor knockdown ECs (Fig. S2 J). Notably, the total number of CFU-GEMMs were significantly decreased after knockdown of either Raptor or Rictor, suggesting a nonredundant role of endothelial mTORC1 and mTORC2 in maintaining HSPC function. Whether each of these complexes regulate distinct attributes of HSPC aging phenotypes in vivo remains to be addressed.

Given the adverse impact of systemic mTOR inhibition on hematopoietic recovery (Fig. 2), we next sought to determine whether EC-specific deletion of *mTOR* influences post-myelosuppressive hematopoietic reconstitution and HSPC recovery. We subjected *mTOR*$^{(ECKO)}$ and littermate controls to myelosuppressive injury (650 Rad) and assessed their hematopoietic recovery (Fig. S3 A). Analysis of peripheral blood revealed that *mTOR*$^{(ECKO)}$ mice displayed a significant delay in hematopoietic recovery, indicating that endothelial mTOR signaling is essential for efficient recovery following myelosuppressive injury (Fig. S3 B). After allowing 28 d for recovery, we assessed total marrow counts per femur and the frequency of phenotypic HSCs and found no significant differences between control and *mTOR*$^{(ECKO)}$ mice (Fig. S3 C). However, progenitor activity, particularly the CFU-GEMM and total CFU counts, was significantly impaired in BM cells derived from *mTOR*$^{(ECKO)}$ mice (Fig. S3 E). We next examined the functional output of the HSPCs of *mTOR*$^{(ECKO)}$ mice at day 28 after myelosuppression by transplanting CD45.2^{+} donor cells from control and *mTOR*$^{(ECKO)}$ mice along with a competitive dose of young CD45.1^{+} WBM in a 5:1 ratio into lethally irradiated young CD45.1 recipients (Fig. S3 F). Long-term, multilineage engraftment was analyzed 4 mo after transplantation, and we found that EC-specific deletion of mTOR resulted in profound defects in engraftment potential following myelosuppressive injury along with an impaired frequency of CD3^{+} T cells (Fig. S3, G and H). Collectively, these data demonstrate that deletion of mTOR signaling within the endothelial niche results in hematopoietic defects that resemble the defects observed during Rapamycin treatment. Additionally, these observations suggest that EC-specific *mTOR* deletion in young mice is sufficient to induce transcriptional, phenotypic, and functional aging of the HSCs at steady state and during regeneration.

To obtain insights into the mechanisms by which endothelial mTOR influences HSPC aging phenotypes, we studied the impact of mTOR deletion on phenotypic and functional characteristics of the BM endothelium (Fig. 5). Deletion of mTOR within the endothelium of young mice did not manifest any gross changes in BM vascular morphology (Fig. 5 A), total number of ECs within the BM (Fig. 5 B), or their apoptosis (Fig. 5 C). mTOR deletion, however, was associated with a modest increase in percentage of ECs in the G0 phase of the cell cycle (Fig. 5 D), consistent with the positive role of mTOR in cell-cycle progression. Notably, *mTOR*$^{(ECKO)}$ mice do not manifest any gross defects in their survival, which is in stark contrast to the deletion of mTOR within hematopoietic cells of adult mice, wherein the mice die within ∼2 wk due to hematopoietic failure (Guo et al., 2013). These findings illuminate the differential tissue-specific roles of mTOR in adult mice; while HSPCs are constantly cycling in order to replenish mature peripheral blood cell output and hence are dependent on active mTOR signaling for cell growth and division, ECs are predominantly quiescent in the adult BM (∼1% of cells are in the SG2M phase). These findings also likely explain the relatively higher degree of toxicity observed with Rapamycin during myelosuppressive recovery compared with steady-state situations, wherein active mTOR signaling is likely to be essential for efficient recovery of both HSPCs and ECs. Collectively, these findings indicate that the HSPC aging phenotypes observed in young *mTOR*$^{(ECKO)}$ mice do not arise from gross vascular disruption but rather are likely due to changes in the instructive signals originating from the endothelial niche.

To address this possibility, we performed transcriptomic analysis on BMECs derived from young control mice, young *mTOR*$^{(ECKO)}$ mice, and aged control mice. The purity of FACS-sorted cells was confirmed by RT-PCR analysis (Fig. 5 E) for expression of *Cdh5* (endothelial identity) and absence of expression of *Ptprc* (hematopoietic identity). We also confirmed the fidelity of the *creERT2* mouse model by performing RT-PCR analysis for the *creERT2* transgene, which demonstrated robust expression within ECs and was not detected in FACS-sorted HSCs (Fig. 5 E). Unsupervised hierarchical clustering of the microarray data revealed that aged ECs demonstrate a unique transcriptional profile compared with that of young control mice and young *mTOR*$^{(ECKO)}$ mice (Fig. 5 F). This indicated that in addition to decreased mTOR signaling, aging is likely associated with changes in multiple signaling pathways and molecular processes within ECs. To gain insights into these processes, we performed a pathway analysis of differentially expressed genes in the aged BM endothelium, which revealed an overrepresentation of senescence-associated secretory pathway and oxidative stress along with a decrease in ubiquitin-proteasome processing and amino acid metabolism pathways (Fig. 5 G). Interestingly,

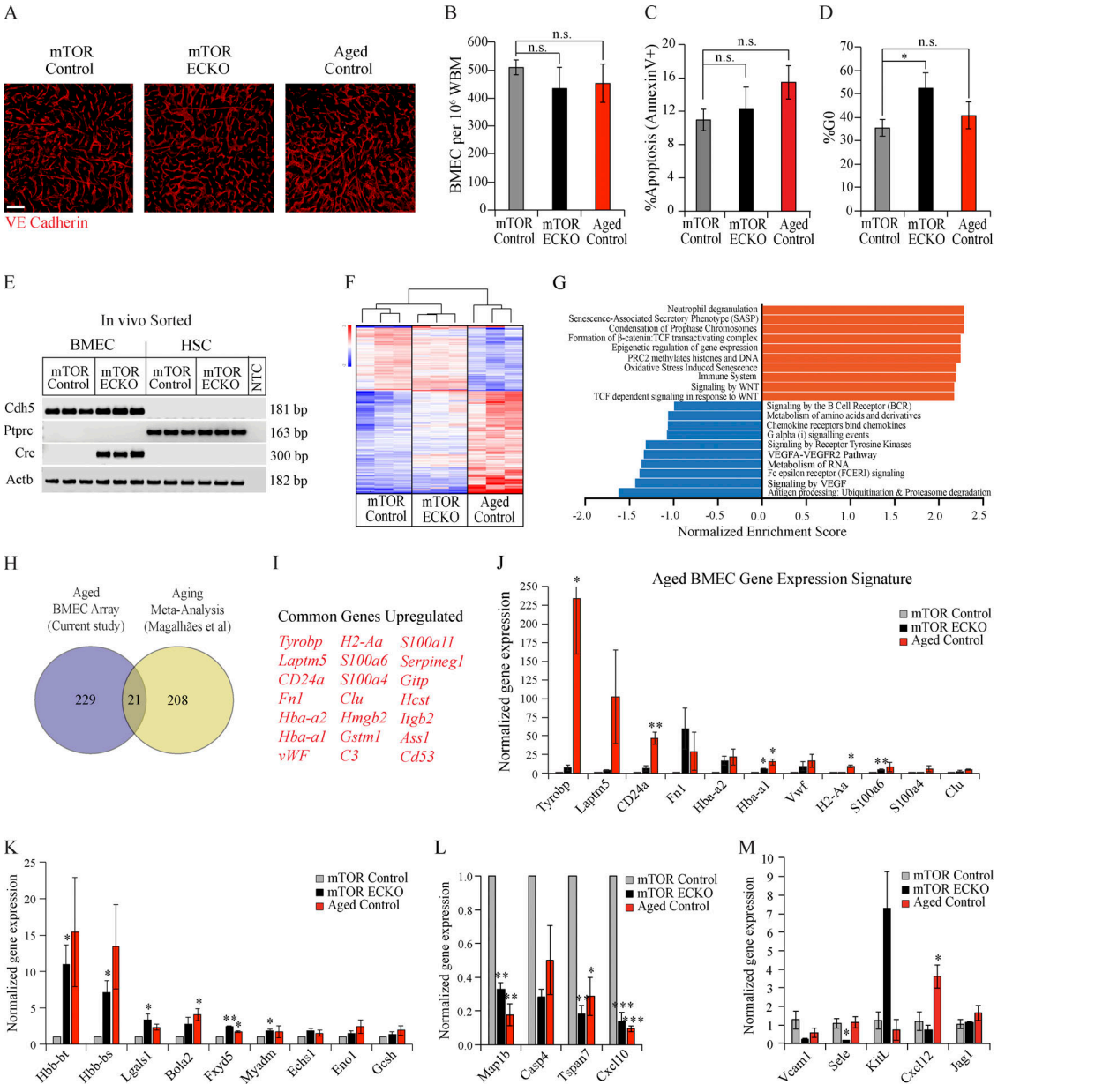

Figure 5. **Loss of endothelial mTOR recapitulates a subset of transcriptional changes observed during physiological aging**. **(A)** Representative immunofluorescence images of femurs intravitally labeled with a vascular-specific VE-cadherin (VECAD) antibody (red) demonstrating normal vascular morphology in *mTOR*$^{(ECKO)}$ mice (n = 4 mice per cohort). Scale bar represents 100 µm. **(B)** Frequency of phenotypic BMECs per 10^6 femur cells assessed by flow cytometry (n = 7 mice per cohort). **(C)** Frequency of apoptotic BMECs (Annexin V$^+$) assessed by flow cytometry (n = 7 mice per cohort). **(D)** Cell-cycle analysis of BMECs (Ki-67/Hoechst staining) assessed by flow cytometry (n = 7 mice per cohort). **(E)** Agarose gel electrophoresis image of RT-PCR amplicons for the indicated genes using RNA isolated from FACS-sorted BMECs and HSCs in the indicated genotypes (n = 3 mice per cohort). Data in A–E represent combined analysis of two independent experiments. **(F)** Transcriptional profiling of BMECs by microarray in the indicated genotypes (n = 3 mice per cohort). **(G)** Reactome Pathway analysis of genes differentially expressed in aged BMECs compared with young BMECs. **(H)** Venn diagram comparing genes showing significant changes between aged BMECs in the current study and a previously published meta-analysis. **(I)** Genes listed demonstrate concordant changes in expression between the current study and published dataset. **(J)** RT-qPCR evaluation of aging-signature genes in BMECs derived from *mTOR*$^{(ECKO)}$ and aged mice (n = 3 mice per cohort). Note: BMECs from *mTOR*$^{(ECKO)}$ mice demonstrate gene expression changes similar to those of aged BMECs. **(K and L)** RT-qPCR evaluation of genes identified to exhibit congruent expression in BMECs derived from *mTOR*$^{(ECKO)}$ and aged mice by microarray (n = 3 mice per cohort). **(M)** RT-qPCR evaluation of known angiocrine factors in BMECs derived from *mTOR*$^{(ECKO)}$ and aged mice (n = 3 mice per cohort). Error bars represent sample mean ± SEM. Statistical significance determined using Student's t test. *, P < 0.05; **, P < 0.01; ***, P < 0.001. n.s., not statistically significant; NTC, no template control.

there was an increase in WNT signaling pathway, which has recently emerged as a regulator of the aging process (Gruber et al., 2016), and a decrease in vascular endothelial growth factor (VEGF) and tyrosine kinase signaling pathways that have been well established as playing key roles in regulating endothelial signaling and likely explain the decreased mTOR signaling in aged BMECs. To define an aging-associated gene expression signature of BM endothelium, we compared the genes that were differentially expressed in aged ECs in our microarray data with a previously published meta-analysis of aging-associated genes (de Magalhães et al., 2009; Fig. 5 H) and identified 21 genes that were commonly up-regulated (Fig. 5 I). Notably, *Hba* has recently been demonstrated to play a key role in regulation of endothelial nitric oxide signaling (Straub et al., 2012), which could potentially impact HSPC function through regulation of shear stress (Pardanaud and Eichmann, 2009).

We next compared the expression of these endothelial aging-signature genes within BMECs derived from young control mice, young $mTOR^{(ECKO)}$ mice, and aged control mice by RT-qPCR analysis (Fig. 5 J). Interestingly, most of these aging-associated signature genes, including *Fn1*, *vWF*, *Hba-a1*, *Hba-a2*, *S100a6*, and *Clu*, demonstrated increased expression in ECs derived from $mTOR^{(ECKO)}$ mice, similar to aged mice (Fig. 5 J). This led to the possibility that aberrant expression of genes commonly altered in ECs of $mTOR^{(ECKO)}$ mice and aged mice, compared with young ECs, could likely reveal candidates that mediate aging-associated HSPC defects. Further analysis of our transcriptome dataset revealed 13 such genes (Fig. 5, K and L), including genes implicated in regulation of cell-matrix interactions (*Lgals1*, *Fxyd5*), metabolism (*Bola2*, *Echs*, *Eno1*, *Gcsh*), and myeloid differentiation of HSPCs (*Myadm*). *Myadm* has recently been shown to regulate endothelial inflammation (Aranda et al., 2013), and increased expression of *Myadm* was observed in mesenchymal stromal cells derived from patients with myeloproliferative neoplasms (Ramos et al., 2017). Since inflammation-associated aging or "inflammaging" has recently emerged as a critical process driving HSPC aging phenotypes, it is likely that genes regulating endothelial inflammation may impact HSPC aging (Kovtonyuk et al., 2016). We also compared the expression of angiocrine factors that are known to regulate HSC function and did not observe any congruent changes in their expression in $mTOR^{(ECKO)}$ mice and aged mice (Fig. 5 M). Collectively, the genes identified by microarray analysis likely represent novel regulators of endothelial niche–HSC interactions and need to be investigated further.

Physiological aging of the HSPC microenvironment results in a decline in the functional potential of HSPCs to reconstitute hematopoiesis, thereby leading to an imbalance of the myeloid/lymphoid ratio, with the skewing toward the myeloid lineage (Ergen et al., 2012; Guidi et al., 2017; Vas et al., 2012). Tipping the balance toward myeloid output can lead to a multitude of age-associated defects, including a significant decline in the body's ability to mount an adaptive immune response coupled with a predisposition toward myeloid neoplasms. Recent studies have indicated the possibility that systemic factors can contribute toward HSPC aging (Ju et al., 2007; Song et al., 2012) and that exposure of aged HSPCs to a young microenvironment can partially rejuvenate their defects (Yamamoto et al., 2018). It has also been demonstrated that aged BMECs have reduced function in regards to regulating hematopoietic niche cells and that it is possible to rejuvenate their functional readout; however, these studies were unable to restore the full functional capacity of the HSPC (Kusumbe et al., 2016). The observation of decreased mTOR signaling within the endothelium of aged mice raises the possibility that activation of mTOR signaling specifically within ECs could alleviate the aging-associated HSPC defects. Future advances in the ability to selectively target the vascular endothelium with pharmacological agents would enable targeted delivery of molecules that activate endothelial mTOR signaling during the aging process, likely leading to improved hematopoietic outcomes.

Concluding remarks

Here, the data presented support the hypothesis that aged BMECs undergo alterations affecting their instructive capacity to properly balance the rate of HSPC maintenance, self-renewal, and differentiation. In particular, changes in BMEC signaling pathways likely contribute to the aging phenotypes seen in the hematopoietic system. This study demonstrates that the AKT/mTOR axis within ECs is critical in preserving HSPC function and that disruption of mTOR signaling specifically in ECs drives pathological phenotypes reminiscent of the hematopoietic defects observed during physiological aging. Furthermore, these data indicate that dissecting the role ECs play in modulating HSPC activity can lead to a better understanding of endothelial contributions in the initiation and progression of many of the common age-related hematopoietic disorders.

Additionally, our data indicate that pharmacological inhibition of mTOR signaling using Rapamycin, a widely regarded rejuvenating agent and clinically used immunosuppressant, has deleterious effects on the aging hematopoietic system, potentially due its adverse impact on the endothelial niche. Aberrant mTOR activation has been observed in a multitude of cancers, and mTOR inhibitors are currently being considered as adjuvant agents for a wide array of hematological malignancies based on promising preclinical evidence (Calimeri and Ferreri, 2017). However, a recent large-scale clinical trial evaluating the efficacy of the mTOR inhibitor everolimus as an adjuvant to post-induction chemotherapy in improving relapse-free survival in acute myeloid leukemia patients was terminated on account of excess mortality in the everolimus cohort (Burnett et al., 2018). Our results indicate that mTOR inhibition has a deleterious impact on hematopoietic recovery following radiation and chemotherapy-induced myelosuppressive injury in aged mice. Collectively, these observations indicate that hematological toxicities of mTOR inhibitors must be carefully considered during evaluation of the potential therapeutic benefit of mTOR inhibitors in rejuvenation strategies targeted toward the elderly patient population.

Materials and methods

Animal use

All murine experiments were conducted in accordance with the Association for Assessment and Accreditation of Laboratory

Animal Care International and National Institutes of Health Office of Laboratory Animal Welfare guidelines and under the approval of the Center for Discovery and Innovation and the Institutional Animal Care and Use Committee. Young and aged C57BL/6 (CD45.2) mice were purchased from the National Institute on Aging and The Jackson Laboratory. Congenic C57BL/6J *mTOR*$^{fl/fl}$ mice (B6.129S4–*Mtor*$^{tm1.2Koz}$/J; Stock no. 011009) were purchased from The Jackson Laboratory and used as described. These mice were backcrossed to C57BL/6 mice for 10 generations by the donating investigator before submission at The Jackson Laboratory. *mTOR*$^{fl/fl}$ mice were maintained by crossing with congenic C57BL/6 mice obtained from The Jackson Laboratory (stock no. 000664). C57BL/6 Tg(*Cdh5-creERT2*)1Rha mice were obtained from Ralf Adams (Max Planck Institute for Molecular Biomedicine, Münster, Germany), and the model was generated in a C57BL/6 background (Benedito et al., 2009). Founder lines were backcrossed to C57BL/6 by the donating investigator for at least five generations. C57BL/6 Tg(*Cdh5-creERT2*)1Rha mice were maintained by crossing with C57BL/6 mice obtained from The Jackson Laboratory (Stock no. 000664). To generate *mTOR*$^{(ECKO)}$ mice, *mTOR*$^{fl/fl}$ mice were crossed with *Cdh5-creERT2* mice. *mTOR*$^{fl/fl}$; *Cdh5-creERT2* mice (8–12 wk) were administered 200 mg/kg tamoxifen (Sigma-Aldrich) via intraperitoneal injection at a concentration of 30 mg/ml in sunflower oil (Sigma-Aldrich) on consecutive 3 d, followed by 3 d off and an additional 3 d of injection. *mTOR*$^{fl/fl}$ Cre-negative littermate mice (8–12 wk) were used as "young mTOR controls." Aged C57BL/6 mice (18–20 mo) were purchased from the National Institute on Aging and The Jackson Laboratory and were allowed to acclimatize in our vivarium for at least 1 mo before experiments and were used as "aged controls." Young and aged control mice received parallel tamoxifen administration along with *mTOR*$^{(ECKO)}$ mice. Experiments were conducted at least 1 mo after tamoxifen administration. B6.SJL-*Ptprc*^{a}*Pepc*^{b}/BoyJ (CD45.1) mice were purchased from The Jackson Laboratory and used as described. For transplantation studies, recipient mice were subjected to 950 Rad of total body irradiation (^{137}Cs) 24 h before transplantation. Transplant recipients were maintained on PicoLab Mouse 20 antibiotic feed (0.025% trimethoprim and 0.124% sulfamethoxazole; LabDiet) for 28 d following irradiation. Microencapsulated Rapamycin feed was prepared according to a previously described protocol (Harrison et al., 2009).

Buffers and media

The following buffers and media were used: (1) magnetic activated cell sorting (MACS) buffer: PBS without Ca^{2+}/Mg^{2+} (pH 7.2; Corning; 21–040-CV) containing 0.5% BSA (Fisher Scientific; BP1605) and 2 mM EDTA (Corning; 46–034-CI); (2) digestion buffer: 1× Hanks Balanced Salt Solution (Life Technologies; 14065) containing 20 mM Hepes (Corning; 25–060-CI), 2.5 mg/ml Collagenase A (Roche; 11088793001), and 1 U/ml Dispase II (Roche; 04942078001); and (3) endothelial growth medium: low-glucose DMEM (ThermoFisher Scientific; 11885–084) and Ham's F-12 (Corning; 10–080; 1:1 ratio), supplemented with 20% heat-inactivated FBS (Denville Scientific; FB5002-H), 1% antibiotic-antimycotic (Corning; 30–004-CI), 1% nonessential amino acids (Corning; 25–025-CI), 10 mM Hepes (Corning; 25–060-CI), 100 µg/ml heparin (Sigma-Aldrich; H3149), and 50 µg/ml EC growth supplement (Alfa Aesar; BT-203).

Peripheral blood analysis

Peripheral blood was collected using 75-mm heparinized glass capillary tubes (Kimble-Chase) via retro-orbital sinus bleeds into PBS (pH 7.2) containing 10 mM EDTA. WBCs, neutrophils, RBCs, and platelet counts were analyzed using an Advia120 (Bayer Healthcare). To quantify steady-state lineage$^+$ hematopoietic cells and mutlilineage HSC engraftment, peripheral blood was depleted of RBCs (RBC Lysis Buffer; Biolegend) according to the manufacturer's recommendations, stained with indicated fluorophore-conjugated antibodies, and analyzed using flow cytometry.

WBM analysis

To quantify total hematopoietic cells, femurs were gently crushed with a mortar and pestle and enzymatically disassociated for 15 min at 37°C in digestion buffer, after which cell suspensions were filtered (40 µm; Corning; 352340) and washed in MACS buffer. Viable cell numbers were quantified using a hemocytometer with Trypan Blue (Life Technologies) exclusion. To quantify HSPCs in the BM, femurs were flushed using a 26.5-gauge needle with MACS buffer. To quantify BMECs (defined as CD45$^-$CD31$^+$ VE-cadherin$^+$ cells), mice were injected retro-orbitally with 25 µg of a fluorophore-conjugated antibody raised against VE-cadherin (Biolegend; BV13) 15 min before sacrifice. Femurs were gently crushed with a mortar and pestle and enzymatically disassociated for 15 min at 37°C in digestion buffer, after which cell suspensions were filtered and washed in MACS buffer. Cells were surface stained using fluorochrome-conjugated antibodies per manufacturer's recommendations. Cell populations were analyzed using flow cytometry.

Flow cytometry and cell sorting

Prior to surface staining, F_c receptors were blocked using a CD16/32 antibody (Biolegend; 93) in MACS buffer for 10 min at 4°C. F_c-blocked samples were stained with fluorophore-conjugated antibodies at the manufacturer's recommended concentrations in MACS buffer for 30 min at 4°C. Stained cells were washed in MACS buffer and fixed in 1% paraformaldehyde (PFA) in PBS (pH 7.2) with 2 mM EDTA for flow cytometric analysis or resuspended in PBS (pH 7.2) with 2 mM EDTA and 1 µg/ml DAPI (Biolegend) for live/dead exclusion and cell sorting. Samples were analyzed using an LSR II SORP (BD Biosciences) and sorted using an ARIA II SORP (BD Biosciences). Data were collected and analyzed using FACS DIVA 8.0.1 software (BD Biosciences).

Phosphoflow cytometry

To assess mTOR phosphorylation, young (12–16 wk) and aged (24 mo) C57BL/6 mice were injected retro-orbitally with 25 µg of fluorophore-conjugated antibody raised against VE-cadherin (BV13) 15 min before sacrifice. Long bones were isolated, crushed, and enzymatically disassociated in digestion buffer for 15 min at 37°C. Resulting cell suspensions were filtered (40 µm) and washed using MACS buffer. Single-cell WBM suspensions

were depleted of lineage-committed hematopoietic cells using a Lineage Cell Depletion Kit (Miltenyi) according to the manufacturer's suggestions. Resulting lineage$^-$ cells were stained with fluorophore-conjugated antibodies raised against CD31 (Biolegend; 390) and CD45 (Biolegend; 30-F11). Stained cells were washed using MACS buffer, fixed, permeabilized using Phosphoflow Fix Buffer 1 and Perm Buffer 3 (BD Biosciences), and stained with antibodies raised against phosphorylated mTOR (Ser2448; BD Biosciences; 563489), phosphorylated AKT (S473; BD Biosciences; 560404), and phosphorylated S6 (S235/236; BD Biosciences; 560434) for 30 min at room temperature according to the manufacturer's recommendations. Cells were washed in MACS buffer. Appropriate concentration-matched isotype controls were used for gating and analysis by flow cytometry.

Cell cycle and apoptosis

Mice were injected retro-orbitally with 25 µg of fluorophore-conjugated antibody raised against VE-cadherin (BV13) 15 min before sacrifice. Long bones were isolated, crushed, and enzymatically disassociated in digestion buffer for 15 min at 37°C. Resulting cell suspensions were filtered (40 µm) and washed using MACS buffer. Single-cell WBM suspensions were surface stained with fluorophore-conjugated antibodies raised against CD31 (390) and CD45 (30-F11). Stained cells were washed in MACS buffer. For cell cycle analysis of BMECs, surface-stained cells were fixed and permeabilized using the BD Cytofix/Cytoperm Kit (BD Biosciences) per manufacturer's suggestions, after which cells were stained with an antibody raised against Ki67 (B56; BD Biosciences; 558616) and counterstained with Hoechst 33342 (BD Biosciences) according to the manufacturer's recommendations. Cells were analyzed by flow cytometry with a low acquisition rate (<500 events per second). Cell-cycle status was classified as G0 (Ki-67^{negative}; 2N DNA content), G1 (Ki-67$^+$; 2N DNA content), and S/G2/M (Ki-67$^+$; >2N DNA content). For evaluation of apoptosis, Annexin V staining was performed on surface-stained cells according to the manufacturer's suggestions (Biolegend; 640906). BMECs that were DAPI$^-$Annexin V$^+$ were defined as apoptotic.

Colony-forming assay

CFUs in semisolid methylcellulose were quantified to assess hematopoietic progenitor activity. WBM was flushed from femurs and tibiae using a 26.5-gauge needle with MACS buffer. Viable cell counts were determined with a hemocytometer using Trypan Blue (Life Technologies). WBM (5×10^4 cells) were plated in duplicate wells of Methocult GF M3434 methylcellulose (StemCell Technologies) according to the manufacturer's suggestions. Colonies were scored for phenotypic CFU-GEMM, CFU-GM, CFU-G, CFU-M, and BFU-E colonies using a SZX16 Stereo-Microscope (Olympus).

BM transplantation assays

To obtain WBM for transplantation studies, long bones (femur and tibia) were flushed using a 26.5-gauge needle with MACS buffer. For HSC transplantation, WBM was depleted of lineage-committed hematopoietic cells using a Lineage Cell Depletion Kit, stained with antibodies raised against SCA1 (Biolegend; D7), cKIT (Biolegend; 2B8), CD150 (Biolegend; TC15-12F12.2), and CD48 (Biolegend; HM48-1), and HSCs (defined as DAPI$^-$ lineage$^-$SCA1$^+$cKIT$^+$CD150$^+$CD48$^-$) were FACS sorted to purity. For primary transplantations, lethally irradiated (950 Rad) CD45.1 recipients (12–16 wk) were injected via retro-orbital sinus with either 100 CD45.2$^+$ phenotypic HSCs or 5×10^5 CD45.2$^+$ WBM cells along with a 5×10^5 CD45.1$^+$ WBM cell competitive dose. Multilineage hematopoietic engraftment after transplantation was monitored by flow cytometry analysis of peripheral blood at the indicated time points by staining with antibodies raised against CD45.2 (Biolegend; 104), CD45.1 (Biolegend; A20), and TER119 (Biolegend; TER119) or CD45.2 (104), GR1 (Biolegend; RB6-8C5), CD11B (Biolegend; M1/70), B220 (Biolegend; RA3-6B2), and CD3 (Biolegend; 17A2). For secondary transplantations, WBM cells from primary recipients were isolated, and 2×10^6 total cells per recipient were injected into either wild-type control or *mTOR*$^{(ECKO)}$ lethally irradiated mice (12–16 wk). Multilineage hematopoietic engraftment after transplantation was monitored by flow cytometry analysis of peripheral blood at the indicated time points.

Transcriptome analysis

For HSC RNA isolation, HSCs were FACS sorted to purity, as described above, into TRIzol LS Reagent (ThermoFisher Scientific). RNA was purified from TRIzol LS according to the manufacturer's recommendations. For BMEC RNA isolation, mice were injected retro-orbitally with 25 µg of a fluorophore-conjugated antibody raised against VE-cadherin (BV13) 15 min before sacrifice. Long bones were isolated, crushed, and enzymatically disassociated in digestion buffer for 15 min at 37°C. Resulting cell suspensions were filtered (40 µm) and washed using MACS buffer. Single-cell WBM suspensions were depleted of lineage-committed hematopoietic cells using a Lineage Cell Depletion Kit according to the manufacturer's suggestions. Resulting lineage$^-$ cells were surface stained with fluorophore-conjugated antibodies raised against CD31 and CD45. Stained cells were washed in MACS buffer. BMECs were sorted to purity into TRIzol LS Reagent. RNA was purified from TRIzol LS according to the manufacturer's recommendations. For gene expression analysis, cDNA was generated and amplified from purified total RNA using the Ovation Pico WTA System V2 (Nugen) according to the manufacturer's suggested protocol. For microarray analysis, amplified cDNA was further fragmented and biotinylated using the Encore Biotin Module (Nugen) according to the manufacturer's recommendations. RNA, amplified cDNA, and fragmented cDNA integrity was confirmed using the Agilent RNA 6000 Nano Kit and 2100 Bioanalyzer. Resulting DNA was hybridized to GeneChip Mouse Gene 1.0 ST Arrays (Affymetrix), labeled with R-Phycoerythrin–conjugated streptavidin, and scanned using the Affymetrix GeneChip Scanner 3000 7G. All liquid handling was performed using an Affymetrix GeneChip Fluidics Station 450. Microarray quality control and gene expression analysis were done using Affymetrix Expression Console and Transcriptome Analysis Console software. To confirm microarray analysis, RT-qPCR analysis was performed using 1 ng amplified cDNA template, 1 µM gene-specific primers, and 1× SYBR Green Master Mix (Applied Biosystems) on a

ViiA7 real-time PCR instrument (Applied Biosystems). Appropriate no-template controls were included in all experiments. Primers were designed in-house or obtained from the Harvard Primer Bank (Spandidos et al., 2010). Primers are listed in Table 1.

Identification of aged HSC and BMEC gene expression signatures

To define a gene expression signature that characterizes an aged HSC, we compared our microarray expression data with previously published microarray datasets (Chambers et al., 2007; Rossi et al., 2005). Using Venny (http://bioinfogp.cnb.csic.es/tools/venny/; Oliveros, 2015), we identified 42 genes showing significant up-regulation and down-regulation within aged HSCs that were common between our study and either of these previous studies, of which 39 genes showed concordant directional changes across the datasets. 37 of the 39 genes had detectable mRNA expression in HSCs by RNA-sequencing (fragments per kilobase per million reads >10; Lis et al., 2017). We confirmed the up-regulation of 10 most abundantly expressed genes by RT-qPCR to define an aged HSC gene expression signature. To define a gene expression signature that characterizes an aged BMEC, we first identified genes that were differentially expressed between young and aged BMECs by using iDEP (Ge et al., 2018). With a false discovery rate cutoff of 0.15 and absolute fold change cutoff of 1.5, we identified 251 genes that were up-regulated and 152 genes that were down-regulated in aged BMECs compared with young BMECs. Reactome Pathway analysis of these differentially expressed genes was performed using WebGestalt (Liao et al., 2019). Since there are no published datasets for aged BMECs, we compared the aging-associated genes in our dataset with a previously published aging meta-analysis (de Magalhães et al., 2009) using Venny and identified 21 genes showing significant up-regulation in our study and the published dataset, and defined it as the aged BMEC gene expression signature. We next identified genes that were differentially expressed between young and mTOR^{ECKO} BMECs by using iDEP. With a false discovery rate cutoff of 0.15 and absolute fold change cutoff of 1.5, we identified 74 genes that were up-regulated and 29 genes that were down-regulated in mTOR^{ECKO} BMECs compared with young BMECs. To identify genes that displayed concordant patterns of expression in aged BMECs and mTOR^{ECKO} BMECs, we compared their list of differentially expressed genes using Venny, which demonstrated 14 genes that were up-regulated and five genes that were down-regulated in both aged BMECs and mTOR^{ECKO} BMECs compared with young BMECs. The 14 up-regulated genes include *Cd24a*, *Fn1*, *Hba-a1*, *Hba-a2*, and *S100a6*, which are part of the aged BMEC gene expression signature. Microarray data have been deposited in ArrayExpress with the accession numbers E-MTAB-8922 and E-MTAB-8923.

Immunocytochemistry

To assess γ-H2AX foci and cellular polarity in HSCs, long bones were flushed using a 26.5-gauge needle with MACS buffer. WBM was depleted of lineage-committed hematopoietic cells using a Lineage Cell Depletion Kit and then surface stained with antibodies raised against SCA1, cKIT, CD150, and CD48, and HSCs were sorted to purity. A minimum of 1,000 sorted HSCs (DAPI$^-$lineage$^-$SCA1$^+$cKIT$^+$CD150$^+$CD48$^-$) were resuspended in 250 µl of MACS buffer; cytospins were performed by applying 250 µl resuspended cells to slides using prewet Shandon Cytoclip, Sample Chambers, and Filter Cards (ThermoFisher Scientific) according to the manufacturer's suggestions. All cytospins were done using the Shandon Cytospin 4 centrifuge with low acceleration at 1,200 rpm for 3 min. HSCs were subsequently air-dried for 20 min on slides, fixed for 10 min in 4% PBS (pH 7.2), rinsed three times for 5 min in PBS (pH 7.2), and incubated in blocking buffer (10% Normal Goat Serum; Jackson ImmunoResearch) and 0.1% Triton X-100 (Sigma-Aldrich) in PBS (pH 7.2) for 30 min at room temperature. Slides were incubated in primary antibody raised against α-Tubulin (Cell Signaling; DM1A) or phospho-H2AX (Ser139; Millipore; JBW301) in blocking buffer overnight at 4°C. Cells were washed three times in PBS (pH 7.2) and incubated in blocking buffer for 1 h with goat anti-mouse IgG (Alexa Fluor 488; Life Technologies) according to the manufacturer's suggestions. Slides were washed three times in PBS (pH 7.2) and stained with DAPI (Biolegend) at 1 µg/ml in PBS (pH 7.2) for 5 min at room temperature. Slides were washed three additional times and mounted in ProLong Gold Antifade Mountant (ThermoFisher Scientific). Cells were imaged on an LSM 710 confocal microscope (Zeiss). A minimum of 50 HSCs were analyzed for each genotype.

To assess BM vascular morphology, mice were intravenously administered 25 µg of Alexa Fluor 647-conjugated VE-cadherin antibody (BV13) via retro-orbital sinus injections. After 15 min, mice were euthanized and cardiac perfused with 4% PFA, after which femurs were isolated, stripped of muscle and connective tissue, and fixed in 4% PFA for 30 min at room temperature. Bones were washed in 1× PBS three times 5 min and cryopreserved in 15% sucrose for 24 h at 4°C and further cryopreserved in 30% sucrose for 24 h at 4°C. Bones were then embedded in a 50% optimal cutting temperature compound (Tissue-Tek) and 50% sucrose solution and flash frozen in liquid nitrogen. Bones were shaved longitudinally on a Leica CM 3050S cryostat to expose the marrow cavity. Shaved bones were unmounted and washed two or three times in 1× PBS until optimal cutting temperature compound was completely melted. Exposed bones were washed three times for 10 min in 1× PBS. 40-µm Z-stack whole mount immunofluorescence images of femurs were acquired on a Nikon C2 confocal laser scanning microscope.

Immunoblot analysis

WBM from long bones (femur and tibia) were flushed using a 26.5-gauge needle with ice-cold PBS (pH 7.2) containing 2 mM EDTA. WBM was depleted of RBCs (RBC lysis buffer) according to the manufacturer's recommendations. Briefly, the flushed marrow cells were pelleted by centrifugation (500 *g* for 5 min at 4°C), and the cells were resuspended in 3 ml of ice-cold 1× RBC lysis buffer, vortexed briefly, and incubated for 5 min on ice. Cells were pelleted by centrifugation (500 *g* for 5 min at 4°C), supernatant was discarded, and cells were washed with 3 ml of ice-cold PBS (pH 7.2). Cell pellets were lysed in radioimmunoprecipitation

Table 1. **List of primers**

Gene	Forward primer (5′–3′)	Reverse primer (5′–3′)	PrimerBank ID
Mt1	AAGAGTGAGTTGGGACACCTT	CGAGACAATACAATGGCCTCC	20072673a1
Mt2	GCCTGCAAATGCAAACAATGC	AGCTGCACTTGTCGGAAGC	33468863a1
Hk2	TGATCGCCTGCTTATTCACGG	AACCGCCTAGAAATCTCCAGA	7305143a1
Itga6	TGCAGAGGGCGAACAGAAC	GCACACGTCACCACTTTGC	31982236a1
Clu	AGCAGGAGGTCTCTGACAATG	GGCTTCCTCTAAACTGTTGAGC	7304967a1
Fyb	TCAACACGGGGAGTAACCC	CGAGCTTTGTCCTGCAACT	2232152a1
Jam2	GTGCCCACTTCTGTTATGACTG	TTCCCTAGCAAACTTGTGCCA	31543010a1
Plscr2	GCTCAGGAACATACTTGCCAG	CAGCATAACCTTCATGTCCAGAT	31982115a1
Sdpr	GCTGCACAGGCAGAAAAGTTC	GTGACAGCATTCACCTGCG	20270267a1
Neo1	TCCAAACACAATAAGCCTGACG	ATGGGACCAAATCTGCATTAACT	112363081c2
Selp	CATCTGGTTCAGTGCTTTGATCT	ACCCGTGAGTTATTCCATGAGT	6755456a1
Slamf1	CAGAAATCAGGGCCTCAAGAG	CACTGGCATAAACTGTGGTGG	29336066a1
Rassf4	CCTATGGGTCTGTGACCAACG	GTAGAGTGCAAACTCACTGGG	30017329a1
Hspa1a	TGGTGCAGTCCGACATGAAG	GCTGAGAGTCGTTGAAGTAGGC	387211a1
Cd24a	GTTGCACCGTTTCCCGGTAA	CCCCTCTGGTGGTAGCGTTA	6753342a1
Tyrobp	GAGTGACACTTTCCCAAGATGC	CCTTGACCTCGGGAGACCA	6755915a1
Hba-a1	GACACTTCTGATTCTGACAGAC	AGAGCCGTGGCTTACATCAA	
Hba-a2	GTGCATGCCTCTCTGGAT	GCAGGCTTCTTCCTACTCAGG	
Laptm5	GATGCCGTACCTCAGGATGG	CTCCCGGTTCTTGACCACG	6754504a1
S100a4	TCCACAAATACTCAGGCAAAGAG	GCAGCTCCCTGGTCAGTAG	53250a1
Fn1	TTCAAGTGTGATCCCCATGAAG	CAGGTCTACGGCAGTTGTCA	19343834a1
Clu	AGCAGGAGGTCTCTGACAATG	GGCTTCCTCTAAACTGTTGAGC	7304967a1
S100a6	CAGTGATCAGTCATGGCATGCC	ACGGTCCCATTTTATTTCAGAGCT	MGI:5780334
Vwf	CTTCTGTACGCCTCAGCTATG	GCCGTTGTAATTCCCACACAAG	33186908a1
H2-Aa	TCAGTCGCAGACGGTGTTTAT	GGGGGCTGGAATCTCAGGT	31981716a1
Hbb-bs	TGTTGACTCACAACCCCAGA	GGCCTTCACTTTGGCATTAC	
Hbb-bt	CTGTTGTGTTGACTTGCAACCT	GGCCTTCACTTTGGCATTAC	
Lgals1	AACCTGGGGAATGTCTCAAAGT	GGTGATGCACACCTCTGTGA	6678682a1
Bola2	GAACTCAGCGCCGATTACCTC	CAGTGGCTTTCCCTCGAACTT	29171318a1
Echs1	TTGTGAACTTGCCATGATGTGT	TGCTCGGGTGAGTCTCTGAG	29789289a1
Gcsh	ATGTCGCTGCAAGTGTCGAG	ACCGTTCCAATACCTTCCTCT	13386066a1
Eno1	TGCGTCCACTGGCATCTAC	CAGAGCAGGCGCAATAGTTTTA	12963491a1
Myadm	ATGCCGGTAACAGTAACTCGT	CCACACAGGTGGATATTAGCTG	8393800a1
Fxyd5	CCAAACCGAGACCCAGCAA	AACTGCCTACACTTCCCACTA	6679168a1
Cxcl10	CCAAGTGCTGCCGTCATTTTC	GGCTCGCAGGGATGATTTCAA	10946576a1
Map1b	TCGCACCGCTTCCTAGACA	CTGGTCCAAGTTGCACTCAAT	6678946a1
Casp4	ACAAACACCCTGACAAACCAC	CACTGCGTTCAGCATTGTTAAA	6671682a1
Tspan7	AGACCAAACCTGTGATAACCTGT	GGGAGCATTTGTGGAGTTCTC	9790005a1
Actb	TGGCACCACACCTTCTACAATGAGC	CCAGAGGCATACAGGGACAGCACAG	
Ptprc	CAGGGTCCACCTACATAAATGCCA	CCTTCTTCACATCGTGTGACCATGAC	
Cre	ATGTCCAATTTACTGACCGTACACCA	ACGATGAAGCATGTTTAGCTGGCCCA	
Cdh5	GAGAGACTGGATTTGGAATCAAATGCAC	CTCATAGGCAAGCACATTCCCTGTG	
Vcam1	GTTCCAGCGAGGGTCTACC	AACTCTTGGCAAACATTAGGTGT	
Sele	ATGCCTCGCGCTTTCTCTC	GTAGTCCCGCTGACAGTATGC	

Table 1. **List of primers (*Continued*)**

Gene	Forward primer (5′–3′)	Reverse primer (5′–3′)	PrimerBank ID
Kitl	GAATCTCCGAAGAGGCCAGAA	GCTGCAACAGGGGGTAACAT	
Cxcl12	TGCATCAGTGACGGTAAACCA	TTCTTCAGCCGTGCAACAATC	
Jag1	CCTCGGGTCAGTTTGAGCTG	CCTTGAGGCACACTTTGAAGTA	

assay (RIPA) buffer (10^7 cells in 0.5 ml RIPA buffer; ThermoFisher Scientific; Cat# 89900) containing 2× Phosphatase Inhibitor (ThermoFisher Scientific; Cat# 78428) and 2× Protease Inhibitor Cocktail (ThermoFisher Scientific; Cat# 78430) for 1 h at 4°C with gentle agitation, sonicated, and centrifuged for 10 min at 21,000 ×*g* at 4°C to remove insoluble debris. Protein concentrations were determined using the DC Protein Assay (BioRad; 5000111), and 20 µg total protein was denatured for 5 min at 70°C in 1× Laemmli Buffer (Sigma-Aldrich; S3401-10VL), resolved on SDS-acrylamide gels, and electroblotted to nitrocellulose. Transferred blots were blocked for 1 h in 5% wt/vol nonfat dry milk in 1× Tris-buffered saline, 0.1% Tween 20 (TBST; Cell Signaling; 9997). Blots were washed three times for 5 min in 1× TBST and incubated overnight at 4°C in 5% BSA wt/vol in 1× TBST with primary antibodies raised against phospho-S6 (Cell Signaling; 4858), S6 (Cell Signaling; 2217), phospho 4EBP-1 (Cell Signaling; 2855), 4EBP-1 (Cell Signaling; 9644), and Actb (Cell Signaling; 4970) at the manufacturer's recommended dilutions. Blots were washed three times for 5 min in 1× TBST and incubated in 5% nonfat dry milk in 1× TBST containing anti-rabbit (H+L) horseradish peroxidase (Jackson ImmunoResearch Laboratories) secondary antibodies at a dilution of 1:20,000 for 1 h at room temperature. Blots were rinsed twice and washed four times for 5 min in 1× TBST and developed using Amersham ECL Prime Western Blotting Detection Reagent (GE Healthcare; RPN2232) according to the manufacturer's suggestions. All blots were developed using Carestream Kodak BioMax Light Film (Sigma-Aldrich).

EC cultures

Primary BMEC cultures were generated from young (8–12 wk) C57BL/6 mice as described previously (Poulos et al., 2017). Briefly, femurs and tibiae were gently crushed using a mortar and pestle and digested with digestion buffer for 15 min at 37°C, filtered (40 µm; 352340), and washed in MACS buffer. WBM was depleted of terminally differentiated hematopoietic cells using a murine Lineage Cell Depletion Kit (Miltenyi Biotec; 130-090-858) according to the manufacturer's recommendations. BMECs were immunopurified from cell suspensions using sheep anti-rat IgG Dynabeads (ThermoFisher Scientific; 11035) precaptured with a CD31 antibody (MEC13.3; Biolegend) in MACS buffer according to the manufacturer's suggestions. CD31 selected BMECs were cultured in endothelial growth media and transduced with 10^4 pg *myrAkt1* lentivirus per 3 × 10^4 ECs. *Akt*-transduced BMECs were selected for 7 d in serum- and cytokine-free StemSpan SFEM (StemCell Technologies Inc.; 09650) media. BMEC lines were stained with antibodies against VE-cadherin, CD31, and CD45 and FACS sorted for purity (BMEC defined as $CD45^-$ $CD31^+$ VE-cadherin$^+$). Established BMEC lines were transduced with GFP-tagged RNA interference (RNAi) lentivirus (BLOCK-iT HiPerform Lentiviral Pol II miR RNAi Expression system; Invitrogen; K4934-00) targeting Raptor or Rictor, and transduced cells were selected by FACS sorting for GFP^+ cells. DNA oligos for generating RNAi expression vectors were designed using the RNAi designer tool (https://rnaidesigner.thermofisher.com/rnaiexpress/; Table 2). A panel of five lentivirus-targeting unique regions within the open reading frames of each gene were screened for identifying lentivirus with the highest efficiency of knockdown. As each individual lentivirus demonstrated ∼20%–30% knockdown of target genes, vectors were redesigned to coexpress two distinct microRNA from a single lentivirus targeting the same gene by a chaining reaction (Invitrogen; K4938-00). Chained RNAi vectors expressing mRaptor_sh_3 and mRaptor_sh_4 (Raptor) and mRictor_sh_1 and mRictor_sh_4 (Rictor) demonstrated >50% knockdown of the respective target genes by immunoblotting analysis and were used for experiments. A chained RNAi vector designed to coexpress microRNA targeting the *Escherichia coli LacZ* gene and a universal negative control sequence (Invitrogen; K4934-00) was used to establish "control" BMEC cell lines. Cell lysates were prepared from established BMEC lines using RIPA buffer. Immunoblotting was performed as described above with primary antibodies raised against phospho-Akt (Cell Signaling; 9271), Akt (Cell Signaling; 4691), phospho 4EBP-1 (Cell Signaling; 2855), 4EBP-1 (Cell Signaling; 9644), Raptor (Cell Signaling; 2280), Rictor (Cell Signaling; 2140), and Tubb (Cell Signaling; 2146) at the manufacturer's recommended dilutions.

BMEC-HSPC co-culture

Primary murine HSPCs were co-cultured on established BMEC lines under serum-free conditions with soluble KIT ligand (sKITL) supplementation, as described previously (Poulos et al., 2016). Briefly, long bones from young C57BL/6J mice (12 wk) were isolated, and WBM was flushed using a 26.5-gauge needle with MACS buffer. WBM was depleted of lineage$^+$ cells using a Lineage Cell Depletion Kit, surface stained using antibodies raised against cKIT and SCA1, and sorted for $lineage^-cKIT^+SCA1^+$ populations. FACS-sorted $lineage^-cKIT^+SCA1^+$ cells (2,500 cells per well) were plated on a single well of a 12-well dish, preplated with BMECs as feeders, in StemSpan SFEM serum-free media with 50 ng/ml recombinant murine sKITL (PeproTech) and split as needed, as previously described (Poulos et al., 2016). Cells were cultured in 37°C and 5% CO_2. All ex vivo expansions were analyzed following 9 d of co-culture. Total $CD45^+$ cell numbers were calculated after 9 d of co-culture by performing flow cytometry. To assess HSPC activity, total co-culture cells were

Table 2. **List of DNA oligos synthesized for generating lentiviral miR RNAi expression vectors**

Name	miR RNAi oligo sequence (5′–3′)
mRaptor_Sh1_top	TGCTGATAAGAGGCGACTGCAGCATCGTTTTGGCCACTGACTGAC**GATGCTGCTCGCCTCTTAT**
mRaptor_Sh1_bottom	CCTGATAAGAGGCGAGCAGCATCGTCAGTCAGTGGCCAAAACGATGCTGCAGTCGCCTCTTATC
mRaptor_Sh2_top	TGCTGAACAGTCGTAGACAAAGATGGGTTTTGGCCACTGACTGAC**CCATCTTTCTACGACTGTT**
mRaptor_Sh2_bottom	CCTGAACAGTCGTAGAAAGATGGGTCAGTCAGTGGCCAAAACCCATCTTTGTCTACGACTGTTC
mRaptor_Sh3_top	TGCTGTAAACAAACTTGCCACGAGCAGTTTTGGCCACTGACTGAC**TGCTCGTGAAGTTTGTTTA**
mRaptor_Sh3_bottom	CCTGTAAACAAACTTCACGAGCAGTCAGTCAGTGGCCAAAACTGCTCGTGGCAAGTTTGTTTAC
mRaptor_Sh4_top	TGCTGATTACAGCAAGAATGAAGGCTGTTTTGGCCACTGACTGAC**AGCCTTCACTTGCTGTAAT**
mRaptor_Sh4_bottom	CCTGATTACAGCAAGTGAAGGCTGTCAGTCAGTGGCCAAAACAGCCTTCATTCTTGCTGTAATC
mRaptor_Sh5_top	TGCTGATTACATTCACAGACTCGGGCGTTTTGGCCACTGACTGAC**GCCCGAGTGTGAATGTAAT**
mRaptor_Sh5_bottom	CCTGATTACATTCACACTCGGGCGTCAGTCAGTGGCCAAAACGCCCGAGTCTGTGAATGTAATC
mRictor_Sh1_top	TGCTGTCATCTTTCTGACTAAGCGAAGTTTTGGCCACTGACTGAC**TTCGCTTACAGAAAGATGA**
mRictor_Sh1_bottom	CCTGTCATCTTTCTGTAAGCGAAGTCAGTCAGTGGCCAAAACTTCGCTTAGTCAGAAAGATGAC
mRictor_Sh2_top	TGCTGAGAACTAGGAAACAAGGAAGCGTTTTGGCCACTGACTGAC**GCTTCCTTTTCCTAGTTCT**
mRictor_Sh2_bottom	CCTGAGAACTAGGAAAAGGAAGCGTCAGTCAGTGGCCAAAACGCTTCCTTGTTTCCTAGTTCTC
mRictor_Sh3_top	TGCTGTACATCAGCTCGCACATACTGGTTTTGGCCACTGACTGAC**CAGTATGTGAGCTGATGTA**
mRictor_Sh3_bottom	CCTGTACATCAGCTCACATACTGGTCAGTCAGTGGCCAAAACCAGTATGTGCGAGCTGATGTAC
mRictor_Sh4_top	TGCTGATTAAGGAGACACTGAAAGACGTTTTGGCCACTGACTGAC**GTCTTTCAGTCTCCTTAAT**
mRictor_Sh4_bottom	CCTGATTAAGGAGACTGAAAGACGTCAGTCAGTGGCCAAAACGTCTTTCAGTGTCTCCTTAATC
mRictor_Sh5_top	TGCTGAATGATTCCCATCTTACTGGCGTTTTGGCCACTGACTGAC**GCCAGTAATGGGAATCATT**
mRictor_Sh5_bottom	CCTGAATGATTCCCATTACTGGCGTCAGTCAGTGGCCAAAACGCCAGTAAGATGGGAATCATTC
mNeg_Sh_top	TGCTGAAATGTACTGCGCGTGGAGACGTTTTGGCCACTGACTGAC**GTCTCCACGCAGTACATTT**
mNeg_Sh_bottom	CCTGAAATGTACTGCGTGGAGACGTCAGTCAGTGGCCAAAACGTCTCCACGCGCAGTACATTTC
LacZ_Sh_top	TGCTGAAATCGCTGATTTGTGTAGTCGTTTTGGCCACTGACTGAC**GACTACACATCAGCGATTT**
LacZ_Sh_bottom	CCTGAAATCGCTGATGTGTAGTCGTCAGTCAGTGGCCAAAACGACTACACAAATCAGCGATTTC

Target sequences are denoted in bold font.

stained with an antibody raised against CD45.2, and 25,000 FACS-sorted CD45.2$^+$ cells were plated in duplicate wells of Methocult GF M3434 methylcellulose according to the manufacturer's suggestions. Colonies were scored for phenotypic CFU-GEMM, CFU-GM, CFU-G, CFU-M, and BFU-E colonies using a SZX16 Stereo-Microscope.

Statistics

Statistical significance was determined using an unpaired two-tailed Student's *t* test, with a significance threshold set at $P < 0.05$. All data are presented as mean, and error bars represent SEM. HSC microarray gene expression significance was determined using Transcriptome Analysis Console software and a conditioned pair ANOVA test with a significance threshold of $P < 0.05$.

Online supplemental material

Fig. S1 shows data demonstrating decreased mTOR signaling in the aged BM microenvironment, including unfractionated WBM cells, lineage$^-$CD45$^+$ hematopoietic cells, and BMECs, and decreased mTOR signaling within BM cells of aged mice following Rapamycin treatment, demonstrates that endothelial-specific expression of the *cre* transgene does not cause hematopoietic defects, and shows that loss of both alleles of endothelial mTOR is essential for inducing HSPC aging phenotypes. Fig. S2 demonstrates that knockdown of either mTORC1 or mTORC2 in cultured ECs impairs their ability to maintain co-cultured HSPCs ex vivo. Fig. S3 shows that endothelial-specific knockout of mTOR results in delayed hematopoietic recovery and HSPC regeneration following a myelosuppressive injury.

Acknowledgments

Our work is supported by the Tri-Institutional Stem Cell Initiative, American Society of Hematology Scholar Award, American Federation of Aging Research Scholar Award, the National Institutes of Health (1R01CA204308, 1R01HL133021, and 1R01AG065436), and the Leukemia and Lymphoma Society. P. Ramalingam is supported by a Glenn/American Federation of Aging Research scholarship for Research in the Biology of Aging. J.M. Butler is a Scholar of the Leukemia and Lymphoma Society.

Author contributions: M.G. Poulos, P. Ramalingam, M.C. Gutkin, L. Katsnelson, A.G. Freire, E. Lazzari, and J.M. Butler

performed experiments and conducted data analyses. P. Ramalingam and J.M. Butler conceived the experiments and wrote the manuscript.

Disclosures: The authors declare no competing interests exist.

Submitted: 2 July 2019
Revised: 18 December 2019
Accepted: 13 March 2020

References

Aranda, J.F., N. Reglero-Real, B. Marcos-Ramiro, A. Ruiz-Sáenz, L. Fernández-Martín, M. Bernabé-Rubio, L. Kremer, A.J. Ridley, I. Correas, M.A. Alonso, and J. Millán. 2013. MYADM controls endothelial barrier function through ERM-dependent regulation of ICAM-1 expression. *Mol. Biol. Cell.* 24:483–494. https://doi.org/10.1091/mbc.e11-11-0914

Armand, P., H.T. Kim, M.M. Sainvil, P.B. Lange, A.A. Giardino, V. Bachanova, S.M. Devine, E.K. Waller, N. Jagirdar, A.F. Herrera, et al. 2016. The addition of sirolimus to the graft-versus-host disease prophylaxis regimen in reduced intensity allogeneic stem cell transplantation for lymphoma: a multicentre randomized trial. *Br. J. Haematol.* 173:96–104. https://doi.org/10.1111/bjh.13931

Balducci, L. 2003. Myelosuppression and its consequences in elderly patients with cancer. *Oncology (Williston Park).* 17(11, Suppl 11):27–32.

Baumgartner, C., S. Toifl, M. Farlik, F. Halbritter, R. Scheicher, I. Fischer, V. Sexl, C. Bock, and M. Baccarini. 2018. An ERK-Dependent Feedback Mechanism Prevents Hematopoietic Stem Cell Exhaustion. *Cell Stem Cell.* 22:879–892.e6: E6. https://doi.org/10.1016/j.stem.2018.05.003

Benedito, R., C. Roca, I. Sörensen, S. Adams, A. Gossler, M. Fruttiger, and R.H. Adams. 2009. The notch ligands Dll4 and Jagged1 have opposing effects on angiogenesis. *Cell.* 137:1124–1135. https://doi.org/10.1016/j.cell.2009.03.025

Bowers, E., A. Slaughter, P.S. Frenette, R. Kuick, O.M. Pello, and D. Lucas. 2018. Granulocyte-derived TNFα promotes vascular and hematopoietic regeneration in the bone marrow. *Nat. Med.* 24:95–102. https://doi.org/10.1038/nm.4448

Burnett, A.K., E. Das Gupta, S. Knapper, A. Khwaja, M. Sweeney, L. Kjeldsen, T. Hawkins, S.E. Betteridge, P. Cahalin, R.E. Clark, et al. UK NCRI AML Study Group. 2018. Addition of the mammalian target of rapamycin inhibitor, everolimus, to consolidation therapy in acute myeloid leukemia: experience from the UK NCRI AML17 trial. *Haematologica.* 103:1654–1661. https://doi.org/10.3324/haematol.2018.189514

Butler, J.M., D.J. Nolan, E.L. Vertes, B. Varnum-Finney, H. Kobayashi, A.T. Hooper, M. Seandel, K. Shido, I.A. White, M. Kobayashi, et al. 2010. Endothelial cells are essential for the self-renewal and repopulation of Notch-dependent hematopoietic stem cells. *Cell Stem Cell.* 6:251–264. https://doi.org/10.1016/j.stem.2010.02.001

Calimeri, T., and A.J.M. Ferreri. 2017. m-TOR inhibitors and their potential role in haematological malignancies. *Br. J. Haematol.* 177:684–702. https://doi.org/10.1111/bjh.14529

Chambers, S.M., C.A. Shaw, C. Gatza, C.J. Fisk, L.A. Donehower, and M.A. Goodell. 2007. Aging hematopoietic stem cells decline in function and exhibit epigenetic dysregulation. *PLoS Biol.* 5:e201. https://doi.org/10.1371/journal.pbio.0050201

Chen, C., Y. Liu, Y. Liu, and P. Zheng. 2009. mTOR regulation and therapeutic rejuvenation of aging hematopoietic stem cells. *Sci. Signal.* 2:ra75. https://doi.org/10.1126/scisignal.2000559

Cho, R.H., H.B. Sieburg, and C.E. Muller-Sieburg. 2008. A new mechanism for the aging of hematopoietic stem cells: aging changes the clonal composition of the stem cell compartment but not individual stem cells. *Blood.* 111:5553–5561. https://doi.org/10.1182/blood-2007-11-123547

Crane, G.M., E. Jeffery, and S.J. Morrison. 2017. Adult haematopoietic stem cell niches. *Nat. Rev. Immunol.* 17:573–590. https://doi.org/10.1038/nri.2017.53

Cutler, C., and J.H. Antin. 2010. Sirolimus immunosuppression for graft-versus-host disease prophylaxis and therapy: an update. *Curr. Opin. Hematol.* 17:500–504. https://doi.org/10.1097/MOH.0b013e32833e5b2e

Cutler, C., N.L. Henry, C. Magee, S. Li, H.T. Kim, E. Alyea, V. Ho, S.J. Lee, R. Soiffer, and J.H. Antin. 2005. Sirolimus and thrombotic microangiopathy after allogeneic hematopoietic stem cell transplantation. *Biol. Blood Marrow Transplant.* 11:551–557. https://doi.org/10.1016/j.bbmt.2005.04.007

Das, A., G.X. Huang, M.S. Bonkowski, A. Longchamp, C. Li, M.B. Schultz, L.J. Kim, B. Osborne, S. Joshi, Y. Lu, et al. 2018. Impairment of an Endothelial NAD^+-H_2S Signaling Network Is a Reversible Cause of Vascular Aging. *Cell.* 173:74–89.e20. https://doi.org/10.1016/j.cell.2018.02.008

de Magalhães, J.P., J. Curado, and G.M. Church. 2009. Meta-analysis of age-related gene expression profiles identifies common signatures of aging. *Bioinformatics.* 25:875–881. https://doi.org/10.1093/bioinformatics/btp073

Decker, M., J. Leslie, Q. Liu, and L. Ding. 2018. Hepatic thrombopoietin is required for bone marrow hematopoietic stem cell maintenance. *Science.* 360:106–110. https://doi.org/10.1126/science.aap8861

Dykstra, B., and G. de Haan. 2008. Hematopoietic stem cell aging and self-renewal. *Cell Tissue Res.* 331:91–101. https://doi.org/10.1007/s00441-007-0529-9

El Assar, M., J. Angulo, S. Vallejo, C. Peiró, C.F. Sánchez-Ferrer, and L. Rodríguez-Mañas. 2012. Mechanisms involved in the aging-induced vascular dysfunction. *Front. Physiol.* 3:132. https://doi.org/10.3389/fphys.2012.00132

Ergen, A.V., N.C. Boles, and M.A. Goodell. 2012. Rantes/Ccl5 influences hematopoietic stem cell subtypes and causes myeloid skewing. *Blood.* 119:2500–2509. https://doi.org/10.1182/blood-2011-11-391730

Flach, J., S.T. Bakker, M. Mohrin, P.C. Conroy, E.M. Pietras, D. Reynaud, S. Alvarez, M.E. Diolaiti, F. Ugarte, E.C. Forsberg, et al. 2014. Replication stress is a potent driver of functional decline in ageing haematopoietic stem cells. *Nature.* 512:198–202. https://doi.org/10.1038/nature13619

Florian, M.C., K. Dörr, A. Niebel, D. Daria, H. Schrezenmeier, M. Rojewski, M.D. Filippi, A. Hasenberg, M. Gunzer, K. Scharffetter-Kochanek, et al. 2012. Cdc42 activity regulates hematopoietic stem cell aging and rejuvenation. *Cell Stem Cell.* 10:520–530. https://doi.org/10.1016/j.stem.2012.04.007

Fok, W.C., Y. Chen, A. Bokov, Y. Zhang, A.B. Salmon, V. Diaz, M. Javors, W.H. Wood III, Y. Zhang, K.G. Becker, et al. 2014. Mice fed rapamycin have an increase in lifespan associated with major changes in the liver transcriptome. *PLoS One.* 9:e83988. https://doi.org/10.1371/journal.pone.0083988

Ge, S.X., E.W. Son, and R. Yao. 2018. iDEP: an integrated web application for differential expression and pathway analysis of RNA-Seq data. *BMC Bioinformatics.* 19:534. https://doi.org/10.1186/s12859-018-2486-6

Geiger, H., G. de Haan, and M.C. Florian. 2013. The ageing haematopoietic stem cell compartment. *Nat. Rev. Immunol.* 13:376–389. https://doi.org/10.1038/nri3433

Gruber, J., Z. Yee, and N.S. Tolwinski. 2016. Developmental Drift and the Role of Wnt Signaling in Aging. *Cancers (Basel).* 8:73. https://doi.org/10.3390/cancers8080073

Guidi, N., M. Sacma, L. Ständker, K. Soller, G. Marka, K. Eiwen, J.M. Weiss, F. Kirchhoff, T. Weil, J.A. Cancelas, et al. 2017. Osteopontin attenuates aging-associated phenotypes of hematopoietic stem cells. *EMBO J.* 36:1463. https://doi.org/10.15252/embj.201796968

Guo, F., S. Zhang, M. Grogg, J.A. Cancelas, M.E. Varney, D.T. Starczynowski, W. Du, J.Q. Yang, W. Liu, G. Thomas, et al. 2013. Mouse gene targeting reveals an essential role of mTOR in hematopoietic stem cell engraftment and hematopoiesis. *Haematologica.* 98:1353–1358. https://doi.org/10.3324/haematol.2012.080424

Harrison, D.E., R. Strong, Z.D. Sharp, J.F. Nelson, C.M. Astle, K. Flurkey, N.L. Nadon, J.E. Wilkinson, K. Frenkel, C.S. Carter, et al. 2009. Rapamycin fed late in life extends lifespan in genetically heterogeneous mice. *Nature.* 460:392–395. https://doi.org/10.1038/nature08221

Hofma, S.H., W.J. van der Giessen, B.M. van Dalen, P.A. Lemos, E.P. McFadden, G. Sianos, J.M. Ligthart, D. van Essen, P.J. de Feyter, and P.W. Serruys. 2006. Indication of long-term endothelial dysfunction after sirolimus-eluting stent implantation. *Eur. Heart J.* 27:166–170. https://doi.org/10.1093/eurheartj/ehi571

Huang, Z., Y. Wu, X. Zhou, J. Qian, W. Zhu, Y. Shu, and P. Liu. 2015. Clinical efficacy of mTOR inhibitors in solid tumors: a systematic review. *Future Oncol.* 11:1687–1699. https://doi.org/10.2217/fon.15.70

Inoki, K., T. Zhu, and K.L. Guan. 2003. TSC2 mediates cellular energy response to control cell growth and survival. *Cell.* 115:577–590. https://doi.org/10.1016/S0092-8674(03)00929-2

Johnson, S.C., M.E. Yanos, A. Bitto, A. Castanza, A. Gagnidze, B. Gonzalez, K. Gupta, J. Hui, C. Jarvie, B.M. Johnson, et al. 2015. Dose-dependent effects of mTOR inhibition on weight and mitochondrial disease in mice. *Front. Genet.* 6:247. https://doi.org/10.3389/fgene.2015.00247

Ju, Z., H. Jiang, M. Jaworski, C. Rathinam, A. Gompf, C. Klein, A. Trumpp, and K.L. Rudolph. 2007. Telomere dysfunction induces environmental

alterations limiting hematopoietic stem cell function and engraftment. *Nat. Med.* 13:742–747. https://doi.org/10.1038/nm1578

Kaeberlein, M., R.W. Powers III, K.K. Steffen, E.A. Westman, D. Hu, N. Dang, E.O. Kerr, K.T. Kirkland, S. Fields, and B.K. Kennedy. 2005. Regulation of yeast replicative life span by TOR and Sch9 in response to nutrients. *Science.* 310:1193–1196. https://doi.org/10.1126/science.1115535

Kapahi, P., B.M. Zid, T. Harper, D. Koslover, V. Sapin, and S. Benzer. 2004. Regulation of lifespan in Drosophila by modulation of genes in the TOR signaling pathway. *Curr. Biol.* 14:885–890. https://doi.org/10.1016/j.cub.2004.03.059

Kennedy, B.K., and D.W. Lamming. 2016. The Mechanistic Target of Rapamycin: The Grand ConducTOR of Metabolism and Aging. *Cell Metab.* 23: 990–1003. https://doi.org/10.1016/j.cmet.2016.05.009

Kobayashi, H., J.M. Butler, R. O'Donnell, M. Kobayashi, B.S. Ding, B. Bonner, V.K. Chiu, D.J. Nolan, K. Shido, L. Benjamin, and S. Rafii. 2010. Angiocrine factors from Akt-activated endothelial cells balance self-renewal and differentiation of haematopoietic stem cells. *Nat. Cell Biol.* 12:1046–1056. https://doi.org/10.1038/ncb2108

Kovtonyuk, L.V., K. Fritsch, X. Feng, M.G. Manz, and H. Takizawa. 2016. Inflamm-Aging of Hematopoiesis, Hematopoietic Stem Cells, and the Bone Marrow Microenvironment. *Front. Immunol.* 7:502. https://doi.org/10.3389/fimmu.2016.00502

Kowalczyk, M.S., I. Tirosh, D. Heckl, T.N. Rao, A. Dixit, B.J. Haas, R.K. Schneider, A.J. Wagers, B.L. Ebert, and A. Regev. 2015. Single-cell RNA-seq reveals changes in cell cycle and differentiation programs upon aging of hematopoietic stem cells. *Genome Res.* 25:1860–1872. https://doi.org/10.1101/gr.192237.115

Kusumbe, A.P., S.K. Ramasamy, T. Itkin, M.A. Mäe, U.H. Langen, C. Betsholtz, T. Lapidot, and R.H. Adams. 2016. Age-dependent modulation of vascular niches for haematopoietic stem cells. *Nature.* 532:380–384. https://doi.org/10.1038/nature17638

Lazzari, E., and J.M. Butler. 2018. The Instructive Role of the Bone Marrow Niche in Aging and Leukemia. *Curr. Stem Cell Rep.* 4:291–298. https://doi.org/10.1007/s40778-018-0143-7

Le Couteur, D.G., and E.G. Lakatta. 2010. A vascular theory of aging. *J. Gerontol. A Biol. Sci. Med. Sci.* 65:1025–1027. https://doi.org/10.1093/gerona/glq135

Lee, J.Y., D. Nakada, O.H. Yilmaz, Z. Tothova, N.M. Joseph, M.S. Lim, D.G. Gilliland, and S.J. Morrison. 2010. mTOR activation induces tumor suppressors that inhibit leukemogenesis and deplete hematopoietic stem cells after Pten deletion. *Cell Stem Cell.* 7:593–605. https://doi.org/10.1016/j.stem.2010.09.015

Liao, Y., J. Wang, E.J. Jaehnig, Z. Shi, and B. Zhang. 2019. WebGestalt 2019: gene set analysis toolkit with revamped UIs and APIs. *Nucleic Acids Res.* 47(W1):W199–W205. https://doi.org/10.1093/nar/gkz401

Lis, R., C.C. Karrasch, M.G. Poulos, B. Kunar, D. Redmond, J.G.B. Duran, C.R. Badwe, W. Schachterle, M. Ginsberg, J. Xiang, et al. 2017. Conversion of adult endothelium to immunocompetent haematopoietic stem cells. *Nature.* 545:439–445. https://doi.org/10.1038/nature22326

Lutz, M., and S. Mielke. 2016. New perspectives on the use of mTOR inhibitors in allogeneic haematopoietic stem cell transplantation and graft-versus-host disease. *Br. J. Clin. Pharmacol.* 82:1171–1179. https://doi.org/10.1111/bcp.13022

Molhoek, K.R., C.C. McSkimming, W.C. Olson, D.L. Brautigan, and C.L. Slingluff Jr. 2009. Apoptosis of CD4(+)CD25(high) T cells in response to Sirolimus requires activation of T cell receptor and is modulated by IL-2. *Cancer Immunol. Immunother.* 58:867–876. https://doi.org/10.1007/s00262-008-0602-6

Neff, F., D. Flores-Dominguez, D.P. Ryan, M. Horsch, S. Schröder, T. Adler, L.C. Afonso, J.A. Aguilar-Pimentel, L. Becker, L. Garrett, et al. 2013. Rapamycin extends murine lifespan but has limited effects on aging. *J. Clin. Invest.* 123:3272–3291. https://doi.org/10.1172/JCI67674

Oliveros, J.C. 2015. Venny. An interactive tool for comparing lists with Venn's diagrams. https://bioinfogp.cnb.csic.es/tools/venny/index.html

Pang, W.W., E.A. Price, D. Sahoo, I. Beerman, W.J. Maloney, D.J. Rossi, S.L. Schrier, and I.L. Weissman. 2011. Human bone marrow hematopoietic stem cells are increased in frequency and myeloid-biased with age. *Proc. Natl. Acad. Sci. USA.* 108:20012–20017. https://doi.org/10.1073/pnas.1116110108

Pardanaud, L., and A. Eichmann. 2009. Stem cells: The stress of forming blood cells. *Nature.* 459:1068–1069. https://doi.org/10.1038/4591068a

Pinho, S., and P.S. Frenette. 2019. Haematopoietic stem cell activity and interactions with the niche. *Nat. Rev. Mol. Cell Biol.* 20:303–320. https://doi.org/10.1038/s41580-019-0103-9

Poulos, M.G., M.J.P. Crowley, M.C. Gutkin, P. Ramalingam, W. Schachterle, J.L. Thomas, O. Elemento, and J.M. Butler. 2015. Vascular Platform to Define Hematopoietic Stem Cell Factors and Enhance Regenerative Hematopoiesis. *Stem Cell Reports.* 5:881–894. https://doi.org/10.1016/j.stemcr.2015.08.018

Poulos, M.G., P. Ramalingam, M.C. Gutkin, M. Kleppe, M. Ginsberg, M.J.P. Crowley, O. Elemento, R.L. Levine, S. Rafii, J. Kitajewski, et al. 2016. Endothelial-specific inhibition of NF-κB enhances functional haematopoiesis. *Nat. Commun.* 7:13829. https://doi.org/10.1038/ncomms13829

Poulos, M.G., P. Ramalingam, M.C. Gutkin, P. Llanos, K. Gilleran, S.Y. Rabbany, and J.M. Butler. 2017. Endothelial transplantation rejuvenates aged hematopoietic stem cell function. *J. Clin. Invest.* 127:4163–4178. https://doi.org/10.1172/JCI93940

Rafii, S., D. Roda, E. Geuna, B. Jimenez, K. Rihawi, M. Capelan, T.A. Yap, L.R. Molife, S.B. Kaye, J.S. de Bono, and U. Banerji. 2015. Higher Risk of Infections with PI3K-AKT-mTOR Pathway Inhibitors in Patients with Advanced Solid Tumors on Phase I Clinical Trials. *Clin. Cancer Res.* 21: 1869–1876. https://doi.org/10.1158/1078-0432.CCR-14-2424

Ramos, T.L., L.I. Sánchez-Abarca, B. Rosón-Burgo, A. Redondo, A. Rico, S. Preciado, R. Ortega, C. Rodríguez, S. Muntión, Á. Hernández-Hernández, et al. 2017. Mesenchymal stromal cells (MSC) from JAK2+ myeloproliferative neoplasms differ from normal MSC and contribute to the maintenance of neoplastic hematopoiesis. *PLoS One.* 12:e0182470. https://doi.org/10.1371/journal.pone.0182470

Rossi, D.J., D. Bryder, J.M. Zahn, H. Ahlenius, R. Sonu, A.J. Wagers, and I.L. Weissman. 2005. Cell intrinsic alterations underlie hematopoietic stem cell aging. *Proc. Natl. Acad. Sci. USA.* 102:9194–9199. https://doi.org/10.1073/pnas.0503280102

Song, Z., J. Zhang, Z. Ju, and K.L. Rudolph. 2012. Telomere dysfunctional environment induces loss of quiescence and inherent impairments of hematopoietic stem cell function. *Aging Cell.* 11:449–455. https://doi.org/10.1111/j.1474-9726.2012.00802.x

Spandidos, A., X. Wang, H. Wang, and B. Seed. 2010. PrimerBank: a resource of human and mouse PCR primer pairs for gene expression detection and quantification. *Nucleic Acids Res.* 38(Database issue, suppl_1): D792–D799. https://doi.org/10.1093/nar/gkp1005

Straub, A.C., A.W. Lohman, M. Billaud, S.R. Johnstone, S.T. Dwyer, M.Y. Lee, P.S. Bortz, A.K. Best, L. Columbus, B. Gaston, and B.E. Isakson. 2012. Endothelial cell expression of haemoglobin α regulates nitric oxide signalling. *Nature.* 491:473–477. https://doi.org/10.1038/nature11626

Tian, L., L. Lu, Z. Yuan, J.R. Lamb, and P.K. Tam. 2004. Acceleration of apoptosis in CD4+CD8+ thymocytes by rapamycin accompanied by increased CD4+CD25+ T cells in the periphery. *Transplantation.* 77: 183–189. https://doi.org/10.1097/01.TP.0000101005.44661.3E

Van Zant, G., and Y. Liang. 2003. The role of stem cells in aging. *Exp. Hematol.* 31:659–672. https://doi.org/10.1016/S0301-472X(03)00088-2

Vas, V., C. Wandhoff, K. Dörr, A. Niebel, and H. Geiger. 2012. Contribution of an aged microenvironment to aging-associated myeloproliferative disease. *PLoS One.* 7:e31523. https://doi.org/10.1371/journal.pone.0031523

Vellai, T., K. Takacs-Vellai, Y. Zhang, A.L. Kovacs, L. Orosz, and F. Müller. 2003. Genetics: influence of TOR kinase on lifespan in C. elegans. *Nature.* 426:620. https://doi.org/10.1038/426620a

Wullschleger, S., R. Loewith, and M.N. Hall. 2006. TOR signaling in growth and metabolism. *Cell.* 124:471–484. https://doi.org/10.1016/j.cell.2006.01.016

Wunderlich, M., B. Mizukawa, F.S. Chou, C. Sexton, M. Shrestha, Y. Saunthararajah, and J.C. Mulloy. 2013. AML cells are differentially sensitive to chemotherapy treatment in a human xenograft model. *Blood.* 121: e90–e97. https://doi.org/10.1182/blood-2012-10-464677

Xu, J., and D. Tian. 2014. Hematologic toxicities associated with mTOR inhibitors temsirolimus and everolimus in cancer patients: a systematic review and meta-analysis. *Curr. Med. Res. Opin.* 30:67–74. https://doi.org/10.1185/03007995.2013.844116

Yamamoto, R., A.C. Wilkinson, J. Ooehara, X. Lan, C.Y. Lai, Y. Nakauchi, J.K. Pritchard, and H. Nakauchi. 2018. Large-Scale Clonal Analysis Resolves Aging of the Mouse Hematopoietic Stem Cell Compartment. *Cell Stem Cell.* 22:600–607.e4: E4. https://doi.org/10.1016/j.stem.2018.03.013

Yan, X., H.A. Himburg, K. Pohl, M. Quarmyne, E. Tran, Y. Zhang, T. Fang, J. Kan, N.J. Chao, L. Zhao, et al. 2016. Deletion of the Imprinted Gene Grb10 Promotes Hematopoietic Stem Cell Self-Renewal and Regeneration. *Cell Rep.* 17:1584–1594. https://doi.org/10.1016/j.celrep.2016.10.025

Zhang, Y., A. Bokov, J. Gelfond, V. Soto, Y. Ikeno, G. Hubbard, V. Diaz, L. Sloane, K. Maslin, S. Treaster, et al. 2014. Rapamycin extends life and health in C57BL/6 mice. *J. Gerontol. A Biol. Sci. Med. Sci.* 69:119–130. https://doi.org/10.1093/gerona/glt056

Zoncu, R., A. Efeyan, and D.M. Sabatini. 2011. mTOR: from growth signal integration to cancer, diabetes and ageing. *Nat. Rev. Mol. Cell Biol.* 12: 21–35. https://doi.org/10.1038/nrm3025

Supplemental material

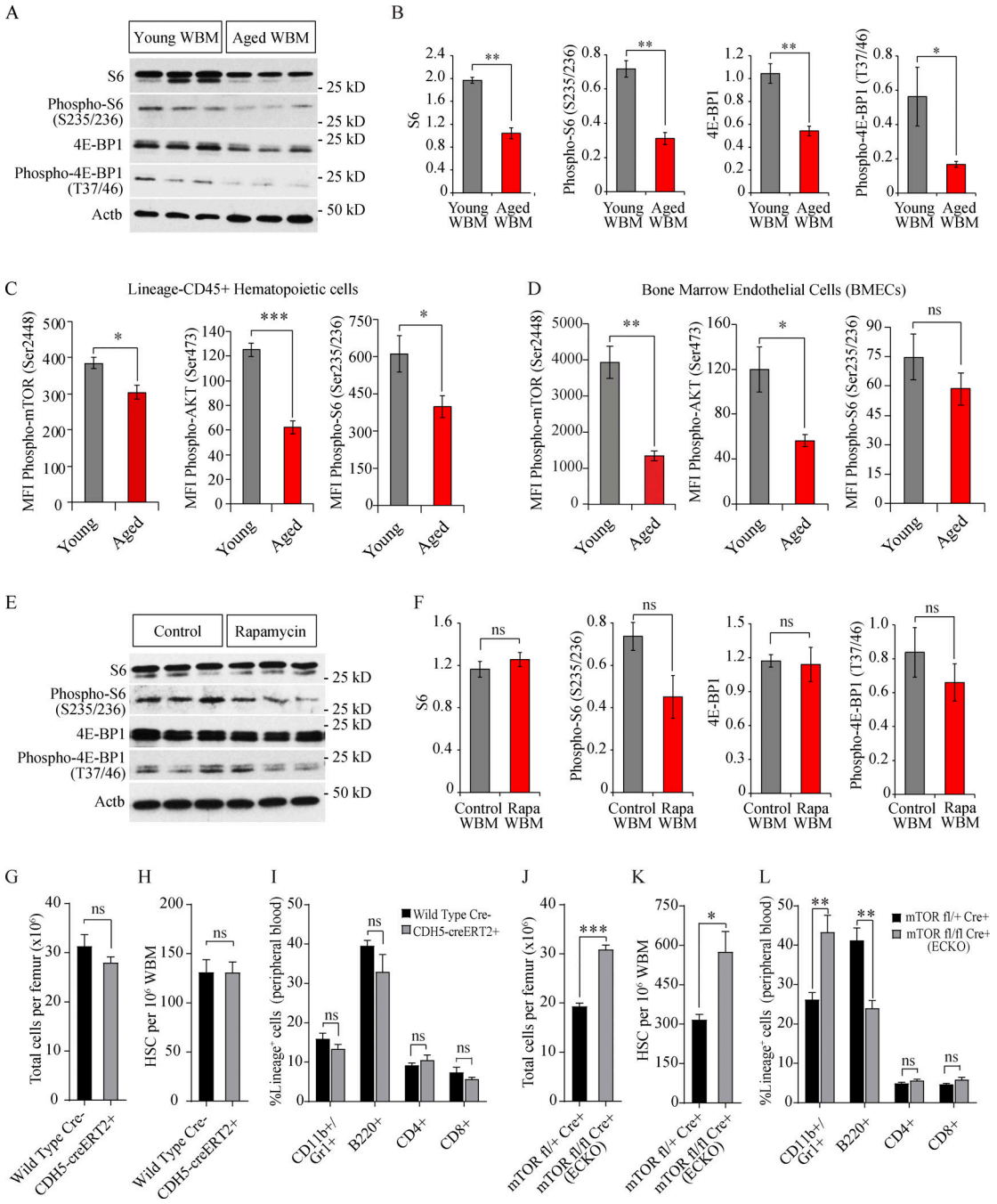

Figure S1. **Aging is associated with decreased mTOR signaling within the BM microenvironment. (A)** Representative immunoblot images demonstrating decreased expression of phospho-S6 and phospho-4EBP-1 in BM cells of aged mice compared with those of young mice. **(B)** Densitometry-based quantification of indicated proteins in the BM of aged mice compared with young mice (n = 6 mice per cohort). Expression of *Actb* was used for normalization. Data represent combined analysis of two independent experiments. **(C and D)** Quantification of mean fluorescent intensity (MFI) of phospho-mTOR (Ser2448), phospho-AKT (Ser473), and phospho-S6 (Ser235/236) by Phosphoflow cytometry in Lin$^-$ CD45$^+$ HSPCs (C) and Lin$^-$ CD45$^-$CD31$^+$VECAD$^+$ BMECs (D; n = 5 mice per cohort). **(E)** Representative immunoblot images demonstrating decreased expression of phospho-S6 and phospho-4EBP-1 in BM cells of aged mice treated with Rapamycin. **(F)** Densitometry-based quantification of indicated proteins in the BM of aged mice treated with Rapamycin compared with aged control mice (n = 3 mice per cohort). Expression of *Actb* was used for normalization. **(G–I)** Analysis of wild-type *cre-* (n = 3) and *Cdh5-creERT2*$^+$ (n = 3) mice revealed no significant differences in BM cellularity (G), HSC frequency (H), and peripheral blood lineage composition (I) indicating that endothelial-specific expression of the *creERT2* transgene does not affect hematopoiesis. **(J–L)** Hematopoietic analysis of heterozygote *mTOR*$^{fl/+}$*creERT2*$^+$ (n = 5) and *mTOR*$^{(ECKO)}$ (n = 5) demonstrated that unlike *mTOR*$^{(ECKO)}$ mice, the littermate heterozygote *mTOR*$^{fl/+}$*creERT2*$^+$ mice do not manifest increased BM cellularity (J), increased HSC frequency (K), and myeloid-skewed peripheral blood lineage composition (L). All mice used in G–L were administered 200 mg/kg tamoxifen via intraperitoneal injection at a concentration of 30 mg/ml in sunflower oil on consecutive 3 d, followed by 3 d off, and an additional 3 d of injection. Note that the same regimen induces HSPC aging phenotypes in homozygote *mTOR*$^{fl/fl}$*cre-ERT2*$^+$ (Fig. 3 and Fig. 4), indicating that loss of both alleles of endothelial *mTOR* is essential to induce HSPC aging phenotypes. Error bars represent mean ± SEM. Statistical significance determined using Student's t test. *, P < 0.05; **, P < 0.01; ***, P < 0.001. ns, not statistically significant; Rapa, Rapamycin.

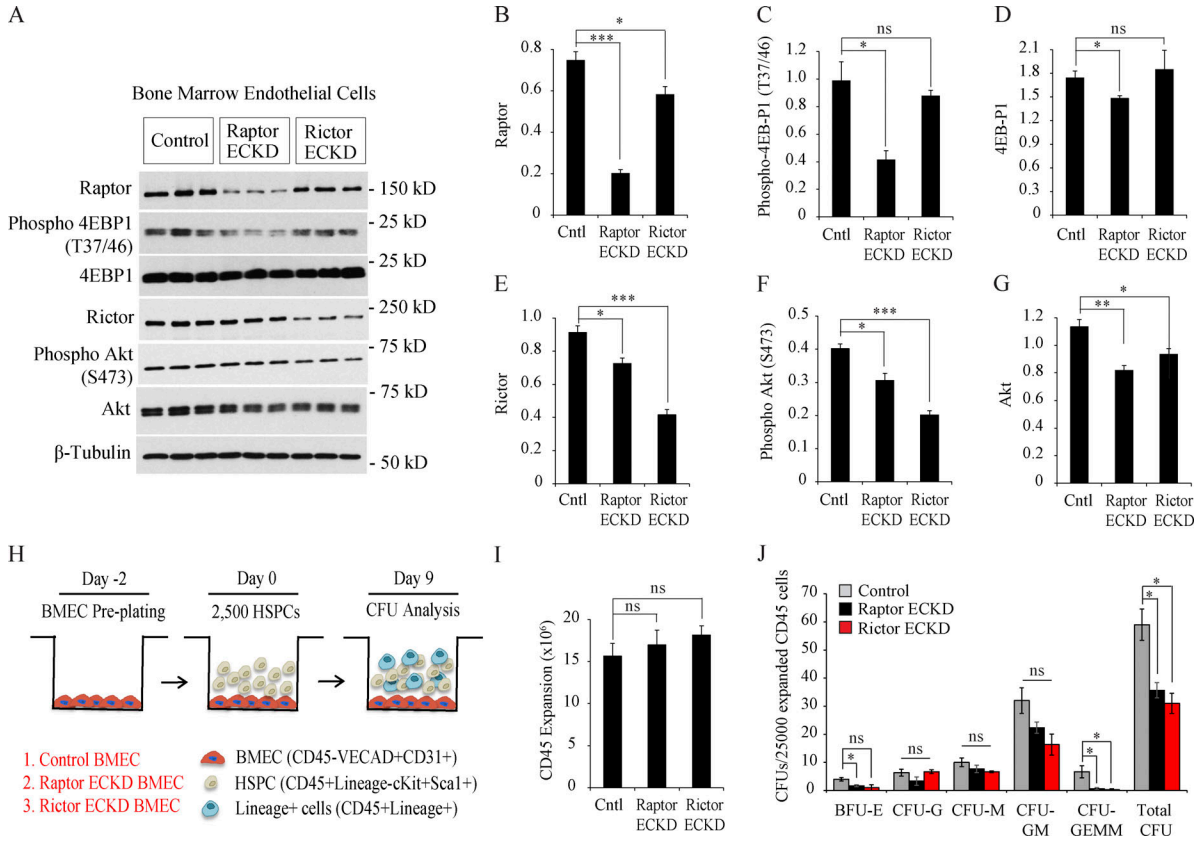

Figure S2. **Endothelial mTORC1 and mTORC2 play nonredundant roles in HSPC maintenance. (A)** Representative immunoblot images demonstrating decreased expression of phospho-4EBP-1 and phospho-Akt in cultured BMECs transduced with lentiviral shRNA targeting Raptor and Rictor, respectively. **(B–G)** Densitometry-based quantification of indicated proteins. Expression of Tubulin was used for normalization. **(H)** Schematic of ex vivo co-culture assay. In short, HSPCs were co-cultured for 9 d with 50 ng/ml sKITL in serum-free media, followed by phenotypic and functional analyses (n = 3 independent co-cultures per genotype). **(I)** Total CD45$^+$ hematopoietic cells estimated by flow cytometry after 9 d of co-culture (n = 3 expansions per genotype). **(J)** Day 9 expanded CD45 cells were FACS purified from feeders. 25,000 CD45$^+$ cells were plated in methylcellulose and scored for CFUs after 8 d (n = 3 per genotype). Data in A–J represent combined analysis of three independent experiments. Error bars represent sample mean ± SEM. Statistical significance determined using Student's t test. *, P < 0.05; **, P < 0.01; ***, P < 0.001. Cntl, control; ECKD, EC cell knockdown; ns, not statistically significant.

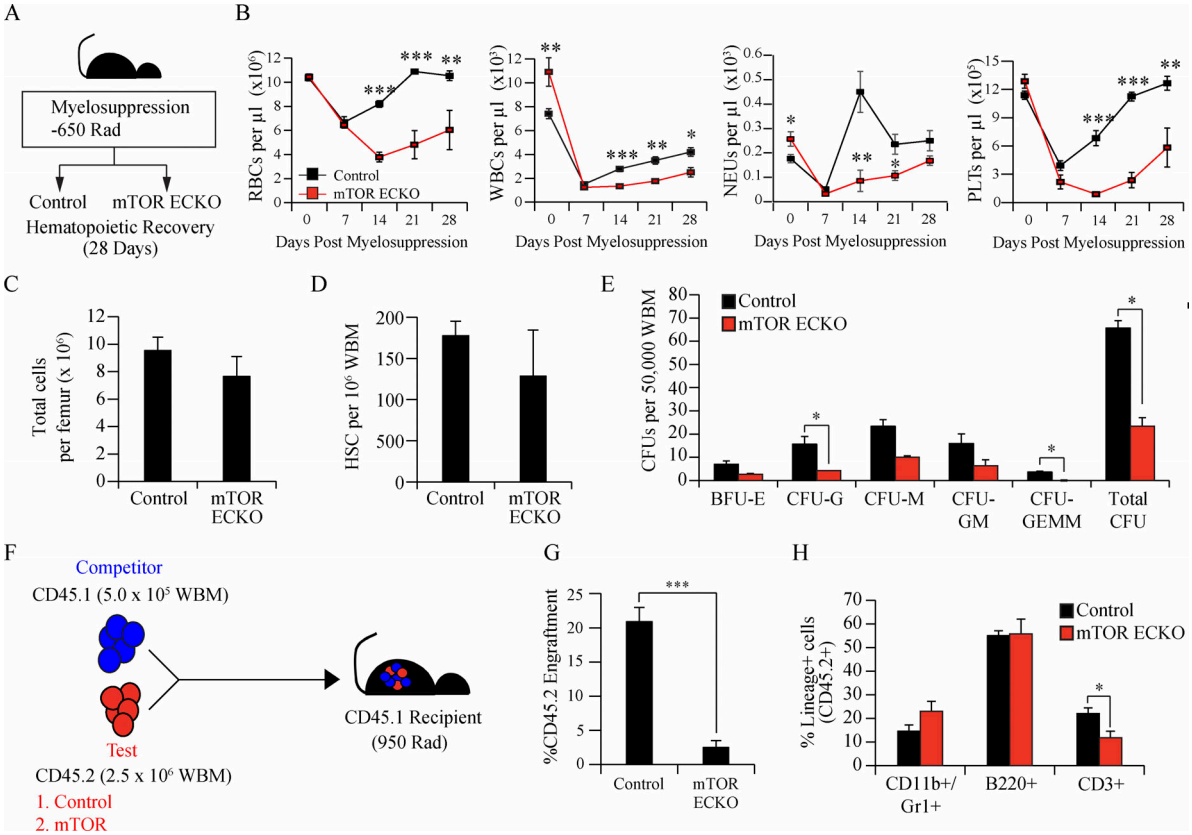

Figure S3. **Loss of endothelial mTOR adversely impacts hematopoietic recovery following myelosuppressive injury. (A)** Experimental design to assess hematopoietic recovery following radiation-induced myelosuppressive injury. **(B)** Peripheral blood counts demonstrate a significant delay in RBC, WBC, and platelet recovery in young *mTOR*$^{(ECKO)}$ mice following radiation (n = 5 mice per cohort). **(C and D)** Total hematopoietic cells per femur (C) and the frequency of HSCs per femur (D; n = 5 per cohort) 28 d after myelosuppressive injury. **(E)** Methylcellulose-based colony assay to assess hematopoietic progenitor activity (n = 3 mice per cohort). Data in B–E represent combined analysis of two independent experiments. **(F)** Schematic of competitive WBM transplantation assay to determine long-term engraftment potential and multilineage reconstitution ability of BM cells following myelosuppressive injury. **(G and H)** Peripheral blood analysis 16 wk after transplantation revealed a loss of long-term engraftment potential (G), along with impaired reconstitution of CD3$^+$ cells (H), in donor BM cells derived from *mTOR*$^{(ECKO)}$ mice (n = 10 recipients per cohort). Data represent average engraftment following transplantation of cells derived from n = 5 independent donor mice per cohort. Error bars represent sample mean ± SEM. Statistical significance determined using Student's t test. *, P < 0.05; **, P < 0.01; ***, P < 0.001. NEU, neutrophil; PLT, platelet.